Available online at www.sciencedirect.com

ScienceDirect

Geochimica et Cosmochimica Acta 238 (2018) 36–54

Geochimica et Cosmochimica Acta

www.elsevier.com/locate/gca

Geochemistry of molybdenum in the continental crust

Allison T. Greaney [a,b,*], Roberta L. Rudnick [a,b], Richard M. Gaschnig [a,c], Joseph B. Whalen [d], Béatrice Luais [e], John D. Clemens [f]

[a] University of Maryland College Park, Department of Geology, College Park, MD 20742, USA
[b] University of California Santa Barbara, Department of Earth Science and Earth Research Institute, Santa Barbara, CA 93106, USA
[c] University of Massachusetts Lowell, Department of Environmental, Earth, and Atmospheric Science, Lowell, MA 01854, USA
[d] Geological Survey of Canada, Central Canada Division, Ottawa, Ontario K1A0E8, Canada
[e] Centre de Recherches Pétrographiques et Géochimiques – CRPG, CNRS - UMR 7358, Université de Lorraine, 54501 Vandoeuvre-les-Nancy Cedex, France
[f] Stellensbosch University, Department of Earth Sciences, Matieland, 7600, South Africa

Received 9 October 2017; accepted in revised form 30 June 2018; Available online 10 July 2018

Abstract

The use of molybdenum as a quantitative paleo-atmosphere redox sensor is predicated on the assumption that Mo is hosted in sulfides in the upper continental crust (UCC). This assumption is tested here by determining the mineralogical hosts of Mo in typical Archean, Proterozoic, and Phanerozoic upper crustal igneous rocks, spanning a compositional range from basalt to granite. Common igneous sulfides such as pyrite and chalcopyrite contain very little Mo (commonly below detection limits of around 10 ng/g) and are not a significant crustal Mo host. By contrast, volcanic glass and Ti-bearing phases such as titanite, ilmenite, magnetite, and rutile contain significantly higher Mo concentrations (e.g., up to 40 μg/g in titanite), and can account for the whole-rock Mo budget in most rocks. However, mass balance between whole-rock and mineral data is not achieved in 4 out of 10 granites analyzed with *in-situ* methods, where Mo may be hosted in undetected trace molybdenite. Significant Mo depletion (*i.e.*, UCC-normalized Mo/Ce < 1) occurs in nearly every granitic rock analyzed here, but not in oceanic basalts or their differentiates (Greaney et al., 2017; Jenner and O'Neill, 2012). On average, granites are missing ~60% of their expected Mo contents. There are two possible reasons for this: (1) Mo partitions into an aqueous magmatic vapor/fluid phase that is expelled from cooling plutons, and/or (2) Mo is partitioned into titaniferous phases during partial melting and fractional crystallization of an evolving magma. The first scenario is likely given the high solubility of oxidized Mo. However, correlations between Mo/Ce and Nb/La in several plutonic suites suggest fractionating phases such as rutile or Fe-Ti oxides may sequester Mo in lower crustal rocks or in subducting slabs in arc settings.

Keywords: Molybdenum; Partitioning; Continental crust; Geochemistry; Molybdenite

1. INTRODUCTION

Molybdenum (Mo) geochemistry has emerged as a powerful tool for tracking early atmospheric oxygenation (e.g., Anbar et al., 2007; Wille et al., 2007; Gaschnig et al., 2014), redox conditions in ocean basins (e.g., Siebert et al., 2003; Arnold et al., 2004; Scott et al., 2008; Dahl et al., 2011), and the influence of subducted sediments and fluids on arc magmas (Freymuth et al., 2015; König et al., 2008). The interest in Mo stems from its geochemical properties: Mo is a multi-valent element whose partitioning behavior depends on the redox state of its environment. Despite the rapidly growing literature on the geochemical

* Corresponding author at: University of California Santa Barbara, Department of Earth Science and Earth Research Institute, Santa Barbara, CA 93106, USA.
E-mail address: greaney@umail.ucsb.edu (A.T. Greaney).

https://doi.org/10.1016/j.gca.2018.06.039
0016-7037/

behavior of Mo at Earth's surface, the behavior of Mo in igneous rocks is less well understood. Yet, such knowledge is crucial for understanding how Mo will behave during crustal weathering and processes that release Mo to sedimentary environments. Additionally, determining the mineralogical hosts of Mo in evolving magmas will lead to a more accurate understanding of Mo behavior during crust formation and differentiation, and the formation of molybdenite deposits in various tectonic settings. This task was first undertaken by Kuroda and Sandell (1954) but, with improved methodology, we aim to expand upon their dataset.

1.1. Properties of Mo

Molybdenum is a geochemically versatile element that displays siderophile (iron/metal-loving; Kuroda and Sandell, 1954; Newsom and Palme, 1984; Lodders and Palme, 1991; Walker, 2016), chalcophile (Goldschmidt, 1937; Kuroda and Sandell, 1954), and lithophile behavior (rock/silicate-loving; Newsom and Palme, 1984; Greaney et al., 2017), depending on the composition of the system of interest (including fO_2 and fS_2), the temperature, and the pressure. Molybdenum's redox sensitivity plays a prominent role in its geochemical behavior because its charge, size, and physical properties change depending on its oxidation state. Molybdenum is insoluble in aqueous fluids when reduced to its tetravalent state, but when oxidized to its hexavalent state it becomes soluble. This relationship between charge and solubility is a key factor in determining the behavior of Mo in the crust and on the Earth's surface.

In igneous systems, the transition from Mo^{4+} to Mo^{6+} occurs over a span of ~10 log units fO_2 (O'Neill and Eggins, 2002), with Mo^{4+} being the dominant state at around three log units below the IW buffer (iron-wüstite) and Mo^{6+} being the dominant state at around one log unit below the FMQ buffer (fayalite-magnetite-quartz). Thus, Mo is expected to exist in its oxidized state in mantle and crustal melts, which have oxygen fugacities near the fayalite-magnetite-quartz (FMQ) or Ni-Ni-oxide (NNO) buffers. The work of Fitton (1995), Zack et al (2002), and subsequent experimental studies suggest that Mo partitions into rutile in eclogites (eclogitic rutile: 2–7 μg/g Mo; Zack et al., 2002), and can be removed from melts generated in subduction zones, even though Mo is found predominately as 6+ in oxidized experimental melts (Holzheid et al., 1994; O'Neill and Eggins, 2002; Bali et al., 2012; Skora et al. 2017). Bali et al. (2012) show that Mo is compatible in rutile in oxidized systems at the NNO buffer (nickel-nickel oxide). This suggests that Mo may be incorporated into rutile even in its oxidized state. Octahedrally-coordinated Mo^{6+} has a similar ionic radius to octahedrally-coordinated Ti^{4+} (59 and 60.5 pm, respectively; Shannon, 1976), so it can replace Ti in a coupled substitution to maintain electrical neutrality. Alternatively, Mo may be locally reduced to Mo^{4+} (ionic radius = 60.5 pm) before exchanging for Ti^{4+} in an isovalent substitution (Zack et al., 2002; Skora et al. 2017). It has also been proposed that Mo is predominately hosted in biotite and amphibole in igneous rocks (Voegelin et al., 2014; Yang et al., 2017), supporting the idea that it follows similar substitution patterns as Ti. However, Mo can also be reduced and incorporated into molybdenite (MoS_2) during oxidation-reduction reactions that occur in hydrothermal ore systems (Stein, 1985).

On the surface of Earth and in oceans, 'free' Mo exists in its oxidized, soluble state given the abundance of atmospheric O_2. Unreactive molybdate (MoO_4^{2-}) is the most common form of Mo in rivers and oceans today, where Mo has a residence time of around 440,000 years (Miller et al., 2011). However, this was probably not the case on early Earth, which lacked or contained only trace concentrations of atmospheric oxygen.

1.2. Molybdenum as a redox proxy

Throughout the first ~2 billion years of Earth's history, the atmosphere was far more reducing than today, probably containing $<10^{-5}$ times the present atmospheric level (PAL) of O_2 (Kasting, 2014 and references therein). Atmospheric oxygen did not accumulate to significant levels until the Great Oxidation Event (GOE), which occurred between 2.4 Ga and 2.3 Ga, when it likely rose to somewhere between 10^{-4} and 10^{-2} PAL (Lyons et al, 2014 and references therein).

Many lines of evidence point to the rise of O_2 during the GOE. Arguably the most important is the disappearance of sulfur-isotope mass-independent fractionation, caused by the creation of an atmospheric ozone shield (Farquhar et al., 2000). Additionally, several redox-sensitive metal proxies (Mo, U, Cr, Re) indicate that oxidative weathering of the continents commenced at or just before the GOE, suggesting that atmospheric O_2 had become sufficiently abundant to cause oxidative weathering of crustal rocks (Anbar et al, 2007; Wille et al., 2007; Scott et al., 2008). These redox-sensitive metals are assumed to be concentrated in minerals that will break down in the presence of atmospheric oxygen, *i.e.,* in sulfides in the case of Mo. Pyrite and molybdenite are commonly invoked as the main Mo sources that contain reduced, insoluble Mo (Anbar et al., 2007, Miller et al., 2011). When these sulfides break down in the presence of atmospheric O_2, the Mo becomes oxidized (and thereby soluble), and can be transported in solution as molybdate (MoO_4^{2-}) in rivers, and eventually the oceans. Once in the ocean, Mo is slowly removed through uptake by Fe-Mn oxides in oxygenated environments, or deposited in black shales within euxinic (high-S, low-O_2) environments. Archean and Proterozoic black shales have been analyzed for Mo and other redox-sensitive elements to track oxidative continental weathering; enrichments suggest oxidative weathering and/or the development of euxinic ocean basins (Turekian and Bertine, 1971; Helz et al., 1996; Erickson and Helz, 2000). High sulfur concentrations are required in the water column for Mo to be reduced and incorporated into Fe-Mo-S phases in reduced oceanic sediments (Helz et al., 1996; Erickson and Helz, 2000). Like Mo, sulfur was probably not abundant in the Archean oceans until atmospheric oxygen caused weathering of continental sulfides during the GOE (Canfield, 2005).

As observed by Gaschnig et al. (2014), Mo enrichments in black shales during and after the GOE are accompanied

by contemporaneous Mo depletions in the UCC. The UCC Mo depletion, relative to the light rare earth elements of similar compatibility (Ce and Pr) first appears in the Paleoproterozoic and continues to the present day. These observations support the hypothesis that oxidative weathering of the continents played a role in removing Mo from the weathered continental crust and transporting it into ocean basins after the GOE.

The use of Mo to trace atmospheric O_2 and infer Precambrian oceanic chemistry is widely accepted in the paleo-atmospheric research community. However, using the Mo concentrations in euxinic sediments to quantify the pO_2 is based on the assumption that Mo is primarily concentrated in sulfides in the UCC, and that these sulfides will break down at a rate that is proportional to pO_2 (Anbar et al., 2007; Williamson and Rimstidt, 1994). While Mo may behave as a chalcophile element in euxinic sedimentary and low-temperature hydrothermal environments, its behavior during igneous differentiation and crust formation is less well understood. Newsom and Palme (1984) suggested that Mo will behave incompatibly during mantle melting, like Ce and Pr, and this is corroborated by the observation that Mo is significantly enriched in the UCC (1.1 μg/g; Rudnick and Gao, 2014) relative to the primitive mantle (0.039 –0.047 μg/g; Greber et al., 2015a, 2015b; Palme and O'Neill, 2004, respectively). Moreover, Mo is observed to behave incompatibly during differentiation of intraplate basalt magmas (Yang et al., 2015; Greaney et al., 2017). Greaney et al. (2017) also showed that while Mo is present in magmatic sulfides (average 2.6 μg/g), it is more abundant in basaltic to andesitic volcanic glasses (average 5 μg/g) and Fe-Ti oxides (average 6.4 μg/g). However, the partitioning behavior of Mo in typical continental crustal igneous rocks, such as granites, has not been systematically studied.

Here, we explore the partitioning of Mo in typical UCC granitic rocks, and incorporate data published on Hawaiian basalts (Greaney et al., 2017), to determine whether Mo is chalcophile, *i.e.,* concentrated primarily in sulfides in the igneous UCC. We present *in-situ* data on Mo concentrations in various minerals as well as whole-rock data on Mo abundances in granitic and basaltic rocks. Our goals are to determine the main mineralogical hosts of Mo in the continental crust and to improve our understanding of the behavior of Mo during crust formation and differentiation.

2. SAMPLES

Granitic rocks are considered to be representative of the felsic UCC, so granitic rocks that span Earth's history form the focus of this study. Since Mo is thought to be generally incompatible during igneous differentiation (Newsom and Palme, 1984), it is expected to be concentrated in more felsic rocks. Given the bimodal composition of the crust, and the hypothesis that the Archean crust may have been significantly more mafic than present-day UCC (e.g., Taylor and McLennan, 1985; Condie, 1993; Dhuime et al., 2015; Gaschnig et al., 2016; Tang et al., 2016), partitioning data from Hawaiian basalts (Greaney et al., 2017) and MORB (Jenner and O'Neill, 2012; Patten et al., 2013) are also considered. We were particularly interested in sampling Archean crust, because its Mo residence and weathering behavior is directly applicable to the GOE. When possible, we selected granitic rocks that retained igneous textures and mineralogy, with an aim of studying previously well-characterized samples. Archean and Proterozoic samples come from the Superior Province (Whalen et al., 2002; Whalen et al., 2003), Baffin Island (Whalen et al. 2012), the Zimbabwe craton (Luais and Hawkesworth, 1994), and the Barberton greenstone belt (Clemens et al., 2006). The majority of these samples are TTGs (tonalite-trondjhemite-granodiorite rocks) that contain higher sodium contents than the more potassic granites that dominate the Proterozoic and Phanerozoic. Additionally, due to the presence of residual rutile or ilmenite in lower-crustal residues and amphibole in mid-crustal residues (Hoffmann et al. 2011), TTG's are generally characterized by a depletion in the high field-strength elements (HFSE) Ti, Nb, and Ta. Complete sample descriptions and photomicrographs can be found in the supplementary materials.

2.1. Barberton TTGs (3.55–3.21 Ga)

Powdered samples of TTGs from the Barberton Greenstone Terrane were analyzed here for whole-rock compositions. No thin sections were available for *in-situ* work. Samples from four generations of plutons that represent distinct tectono-magmatic events were studied: the 3.55–3.49 Ga Steynsdorp pluton; the 3.46–3.42 Ga Stolzburg, Doornhoek, Theespruit, and Erstehoek plutons; the 3.29–3.24 Ga Badplaas pluton; and the 3.24–3.23 Ga Nelshoogte pluton (Clemens et al., 2006; Moyen et al., 2007; Kröner et al., 1991). The Barberton Terrane is one of the most intensively studied suites of Archean TTGs in the world, and several interpretations have been developed to explain the petrogenesis of the TTGs and greenstone belts. A consensus has developed around the hypothesis that these plutons were emplaced during accretion of an exotic terrane and subsequent post-orogenic collapse (Clemens et al., 2006; Moyen et al., 2007).

2.2. Superior Province TTGs (3.0–2.7 Ga)

The TTGs from the Superior Province come from the North Caribou Terrane plutonic complex (~3.0 Ga; Whalen et al., 2003) and the Central Wabigoon subprovince (~2.7 Ga; Whalen et al., 2002). The North Caribou samples are mainly derived from the English Lake Plutonic Suite and range in composition from felsic tonalites and trondhjemites to amphibolitic and pyroxenitic xenolithic enclaves that may have originated as cumulates. Geochemical modeling suggests a genetic link between the cumulate enclaves and the TTGs, and an overall hydrous source for this suite. The younger Central Wabigoon samples are classified as granite to granodiorite and have a higher K_2O/Na_2O ratios than the North Caribou TTGs. This suite is thought to have formed from the partial melting of over-thickened lower crust during the collision of arcs, such as the one that potentially produced the North

Caribou samples. Both whole-rock and *in-situ* data were collected for this suite. Three samples were sectioned for *in-situ* analysis. These are composed of quartz, plagioclase, K-feldspar, biotite, amphibole (primarily hornblende), titanite, Fe-Ti oxides, and minor muscovite and sulfides (Fig. 1), all of which were analyzed for Mo concentration.

2.3. Zimbabwe Craton TTGs (2.9–2.6 Ga)

The samples from the Zimbabwe craton are mainly tonalites from the 2.9 Ga Mashaba suite, as well as two samples from the 2.6 Ga Chibi Granite. The Zimbabwe craton is bounded by three belts that accreted between the Neoarchean Limpopo Belt and the Neoproterozoic Zambezi and Mozambique Belts. The craton itself is composed of 2.8–2.5 Ga greenstone sequences and 3.5–2.9 Ga TTGs. Luais and Hawkesworth (1994, 2002) outline a petrogenetic model that involves partial melting of a garnet-bearing amphibolite and subsequent fractional crystallization to produce the TTG suites. In this model, the Mashaba tonalite was formed by direct fusion products of basaltic protolower crust leaving a garnet amphibolite residue. The late Chibi granite is interpreted to have been derived through partial melting of greenstone mafic volcanic rocks (Hawkesworth et al., 1979). Partial melting in the deeper part of a thick crust has been invoked to explain the formation of these units (Hawkesworth et al., 1979; Luais and Hawkesworth, 1994, 2002). Whole-rock and *in-situ* data were collected for this suite, and data for major and trace elements were previously published in Luais and Hawkesworth (1994). The four samples selected for *in-situ* analysis are variably foliated and contain alteration products such as chlorite, cummingtonite, epidote, and sericite. Common phases are quartz, plagioclase, K-feldspar, biotite, hornblende, muscovite, titanite, Fe-Ti oxides, apatite, and zircon.

2.4. Baffin Island (1.88 Ga)

Whole-rock powders from the Qikiqtarjuaq Plutonic Suite (QPS) show the largest compositional range of all suites studied here, varying from granodiorite/tonalite to gabbro (Whalen et al., 2012). These intrusive bodies form a portion of the Cumberland batholithic complex on Baffin Island. The origin of the QPS is uncertain, as it is a relatively newly discovered and analyzed unit. However, U-Pb ages suggest that it is ~35 Myr older than the Cumberland Batholith (Rayner et al., 2012), which has been interpreted to be a Trans-Hudson Orogeny post-accretionary batholith, possibly resulting from a delamination event from the base of over-thickened crust (Whalen et al., 2010). Thus, it can be inferred that the QPS was emplaced at the initiation of an accretionary event, and may be arc-derived. Data for all major and trace elements

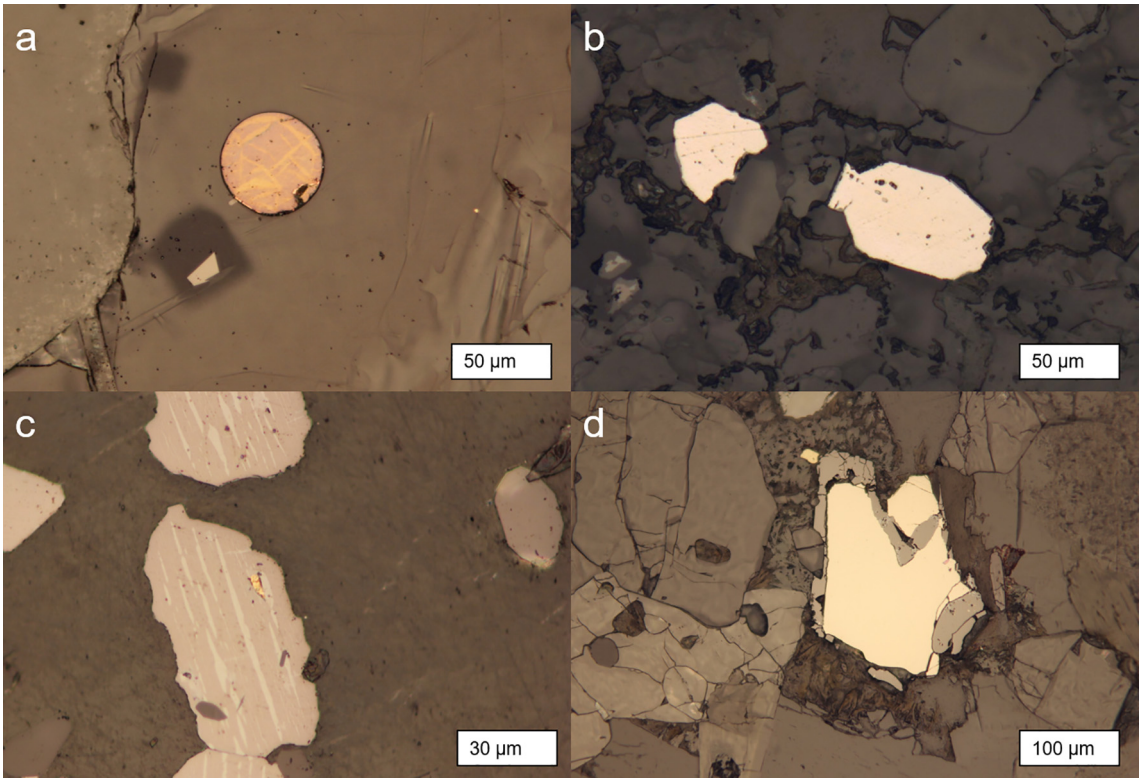

Fig. 1. Photomicrographs of sulfides targeted for laser ablation analysis. (A) Immiscible sulfide bleb from the Kilauea Iki lava lake (KI67-3-76.2) showing needle-like exsolution textures. A second minute (≤1 µm diameter) sulfide is visible on the right. (B) Pyrite from the Archean Superior province tonalite (WXP99-119). (C) Small chalcopyrite inclusion (yellow) hosted in magnetite having ilmenite exsolution from a Mesozoic granite (10RMG005). (D) Pyrite rimmed by magnetite from the Paleozoic Ellicott City Granodiorite (AG1401). (For interpretation of the references to color in this figure legend, the reader is referred to the web version of this article.)

were previously published in Whalen et al. (2012), but Mo concentrations were re-analyzed in this study using a more precise standard-addition technique. No thin sections were analyzed.

2.5. Phanerozoic granites

Mesozoic granitic rocks from the Western USA (Gaschnig et al., 2011, Gaschnig et al., 2017a, 2017b) and a Silurian granite from the Eastern US were analyzed as well. These include a garnet-bearing peraluminous granite from the Idaho batholith, a metaluminous tonalite from the Lookout Mountain pluton in the Blue Mountains (Oregon and Idaho, USA), and a Neo-Acadian epidote-bearing granodiorite (Ellicott City Granodiorite, Maryland, USA). These samples consist of common granitic minerals – abundant feldspar, quartz, biotite, and amphibole with accessory muscovite, titanite, epidote, magnetite, ilmenite, apatite, allanite, zircon, and sulfides (Fig. 1, see supplementary sample descriptions). Whole-rock and *in-situ* analyses of thin sections were carried out on these samples.

2.6. Kilauea Iki lavas

Data from the Kilauea Iki lava lake, Hawaii, reported in Greaney et al. (2017), are considered here for a more complete assessment of mineralogical hosts of Mo. The lava lake erupted in 1959 and is considered a prime natural laboratory for studying basaltic magma differentiation. Samples ranging through the entire differentiation suite from 43.7 to 57.1 wt% SiO_2 were subjected to whole-rock and *in-situ* analysis. The rocks contain olivine, pyroxene (augite), plagioclase, Fe-Ti oxides, glass, and minor apatite and sulfides (Fig. 1).

3. METHODS

The methods follow those of Greaney et al. (2017) and Gaschnig et al. (2015), and are reproduced here in detail in the supplementary material. Whole-rock trace element analyses were carried out by standard-addition solution inductively coupled plasma mass spectrometry (ICP-MS). Samples were dissolved in high pressure PTFE bombs using HF/HNO3, then three aliquots were spiked with variable known amounts of Mo using spikes created by Gaschnig et al. (2015). This method produces a calibration curve from the sample itself, instead of having to extrapolate a calibration curve from external standards, which could induce errors associated with the extrapolation and improperly calibrated standards. The sample aliquots were analyzed on an Element2 HR-ICP-MS at the University of Maryland in MR and LR mode for three isotopes of Mo (95, 97, and 98). The limit of detection (LOD) ranged from 0.03 μg/g to 0.10 μg/g for most analytical sessions. However, it was as high as 0.16 μg/g during analyses of the Barberton suite TTGs. The variable LOD is reflected in Table 1. The reported Mo abundances for the three isotopes never varied by more than the reported RSD calculated from the counting statistics. USGS standard reference rock powders AGV-2 and BHVO-1 were dissolved alongside each batch of samples and run as secondary standards (Table 2). AGV-2's external reproducibility results in a 2RSD of 7%. BHVO-1 (2RSD ~ 25%) is notoriously difficult to reproduce (Willbold et al., 2016; Gaschnig et al. 2015), possibly due to heterogeneities in the sample powder.

In addition, to demonstrate the robustness of measuring low-Mo abundances with the standard addition method, three low-[Mo] TTGs from different suites were redissolved and analyzed by isotope dilution at the Arizona State University Keck Biogeochemistry Lab. Two of the three samples show excellent reproducibility, while the isotope-dilution data gave even lower Mo abundances for the third sample, ZB89-10 (0.13 μg/g by ID vs. 0.25 μg/g by standard addition). This discrepancy may reflect a slightly heterogeneous powder due to nuggets of a Mo-rich phase, given that mass balance was not achieved for this sample (see Section 4.1.3 and Table S4), and a Mo-rich phase was observed within magnetite of another sample from this same TTG suite (see Section 4.1.1). These replicate data are reported in the online supplement. Additionally, for most plutonic suites, a full suite of trace elements were analyzed, including Ga, Ge, Cd, In, Sn, Sb, W, Tl, and Bi. These data are provided in the supplementary materials.

In-situ mineral data were collected using electron probe microanalysis (EPMA) followed by laser ablation ICP-MS using a New Wave UP-213 nm laser attached to an Element2 HR-ICP-MS at the University of Maryland and a Photon Machines 193 nm laser attached to an Agilent 7700x Quadropole ICP-MS at the University of California Santa Barbara. NIST-610 was the external standard, and the glasses BHVO-2g and NIST-612, as well as a synthetic Mo-bearing sulfide produced by James Brenan (formerly at the University of Toronto, now at Dalhousie University) were analyzed as secondary standards (Table 2). Spot-sizes ranged from 25 μm (for smaller sulfides) to 80 μm (for silicates and larger sulfides). Three isotopes of Mo were measured (95, 97, and 98), with all returning values that fell within the error calculated by counting statistics, except when an obvious interference was present (e.g., $^{55}Mn^{40}Ar$ on ^{95}Mo in garnet). Abundances of ^{98}Mo are therefore reported for the *in-situ* data. The LOD for *in-situ* Mo analyses ranges were typically ~0.01 μg/g, however they occasionally ranged as high as 0.1 μg/g, depending on the analyte/background ratio of the instrument that day. The LA-ICP-MS data were processed using Iolite (Paton et al. 2011).

4. RESULTS

4.1. *In-situ* data

4.1.1. Sulfides

A total of 78 sulfide grains were analyzed from the Phanerozoic granites, TTGs, and several evolved samples from the Kilauea Iki lava lake, Hawaii. Pyrite, chalcopyrite, and pyrrhotite are present in the granitic samples while the sulfide blebs in the Kilauea Iki lavas form solid solutions between isocubanite and bornite (see Greaney et al., 2017

Table 1
Samples analyzed for whole-rock (WR) [Mo] and in-situ [Mo]. SA = standard addition ICP-MS; LA = laser ablation ICP-MS; MB = mass balance attained? (yes or no). The SiO_2 (measured by the listed reference) and Mo values given are for the whole rock with 2σ representing internal error. Three samples were replicated by isotope dilution and those values are designated as "rep". Complete whole rock major and trace element data can be found in the supplementary information.

Sample	Unit/Pluton	Age, Ga	Rock type	Analysis	MB	SiO_2	Mo (μg/g)	2σ	Reference
Barberton									
NLG1	Nelshoogte	3.24–3.23	TTG	SA		70.1	0.34	0.01	Clemens et al. (2006); Ages from
NLG14	Nelshoogte	3.24–3.23	TTG	SA		NA	0.38	0.01	Moyen et al. (2007)
NLG15	Nelshoogte	3.24–3.23	TTG	SA		63.1	0.48	0.04	
NLG25A	Nelshoogte	3.24–3.23	TTG	SA		71.1	0.32	0.02	
BDP5A	Badplaas	3.29–3.24	TTG	SA		70.5	<0.16	–	
BDP5C	Badplaas	3.29–3.24	Tonalite dyke	SA		72.8	0.17	0.01	
BDP8A	Badplaas	3.29–3.24	TTG	SA		74	0.18	0.01	
EHK1	Eerstehoek	3.46–3.42	TTG	SA		72.4	<0.16	–	
TH4A	Theespruit	3.46–3.42	TTG	SA		70.3	0.20	0.01	
DNK1	Doornhoek	3.46–3.42	TTG	SA		74	0.23	0.01	
STZ1	Stolzburg	3.46–3.42	TTG	SA		70.7	0.48	0.09	
STZ17	Stolzburg	3.46–3.42	TTG	SA		71.6	0.34	0.09	
STY1	Steynsdorp	3.55–3.49	TTG	SA		65.7	0.16	0.04	
STY1 rep							0.14	0.01	
STY3A	Steynsdorp	3.55–3.49	TTG	SA		72.9	0.16	0.05	
STY4B	Steynsdorp	3.55–3.49	TTG	SA		75.1	<0.16	–	
Zimbabwe									
Zb89-53	Chibi	2.7–2.6	Granite	SA, LA	No	72	0.84	0.04	Luais and Hawkesworth (1994)
Zb89-57	Chibi	2.7–2.6	Granite	SA		74.8	0.26	0.01	
ZB89-10	Mashaba I	2.9	Tonalite	SA, LA	No	71	0.25	0.02	
ZB89-10 rep							0.13	0.01	
ZB89-11	Mashaba I	2.9	Tonalite	SA		67.3	0.07	0.02	
Zb89-12	Mashaba I	2.9	Tonalite	SA		69.4	0.14	0.01	
Zb89-13	Mashaba I	2.9	Tonalite	SA, LA	Yes	68.5	0.20	0.03	
Zb89-15	Mashaba I	2.9	Tonalite	SA, LA	Yes	70.5	0.13	0.02	
Zb89-46	Mashaba I	2.9	Tonalite	SA		70.1	0.07	0.02	
Rh75-Mt7	Mashaba I	2.9	Tonalite	SA		71.2	0.05	0.01	
Superior									
WXP99-119	N. Caribou	2.999	Tonalite	SA	No	63.7	0.16	0.01	Whalen et al. (2002, 2003)
WXP99-123	N. Caribou	2.999	Tonalite	SA, LA	Yes	62.6	0.14	0.01	
WXP99-138	N. Caribou	2.999	Quartz diorite	SA	No	61.7	0.21	0.01	
WXP99-176	N. Caribou	3.006	Trondhjemite	SA, LA		72.1	0.32	0.02	
WXP99-129	N. Caribou	2.999	Tonalite	SA		62.5	nd	–	
WXP 99–139	N. Caribou	NA	Quartz diorite	SA		63.8	<0.10	–	
WXP 99–143	N. Caribou	NA	Quartz diorite	SA		60.7	<0.10	–	
WXP 99–143 rep							0.11	0.01	
WXP 99–145	N. Caribou	2.992	Gabbro enclave	SA		49.3	0.90	0.05	
PBA99-2064c	N. Caribou	NA	Gabbro enclave	SA		46.1	<0.10	–	
PBA99-2072c	N. Caribou	NA	Amph-lite encl.	SA		50.1	0.13	0.02	
PBA99-2072e	N. Caribou	NA	Pyx-ite encl.	SA		45.2	0.17	0.02	
PBA97-23	C. Wabigoon	2.72–2.71	Granite	SA, LA	Yes	71.3	0.32	0.02	
PBA97-319	C. Wabigoon	2.72–2.71	Granodiorite	SA		69.6	0.17	0.01	

(*continued on next page*)

Table 1 (*continued*)

Sample	Unit/Pluton	Age, Ga	Rock type	Analysis	MB	SiO_2	Mo (μg/g)	2σ	Reference
Baffin Island									
10SRB-Y199B-01	QPS	1.88	Quartz gabbro	SA		50.3	2.91	0.49	Whalen et al. (2012)
10SRB-Y201A-02	QPS	1.88	Granodiorite	SA		64.2	2.27	0.38	
10SRB-Y202A-01	QPS	1.88	Syenogranite	SA		70.6	0.53	0.09	
10SRB-Y204A-02	QPS	1.88	Monzogranite	SA		67.3	0.60	0.10	
10SRB-M295A-01	QPS	1.88	Monzogranite	SA		72.3	0.11	0.02	
10SRB-R301A-01	QPS	1.88	Granodiorite	SA		65.1	2.10	0.35	
Phanerozoic									
AG1401	Ellicott City Gd.	460 Ma	Granodiorite	SA, LA	Yes	61.6	0.17	0.02	
07RMG52	Idaho Bath.	80 Ma	Granite	SA, LA	No	74.5	0.45	0.02	
10RMG005	Lookout Mtn	124 Ma	Tonalite	SA, LA	No	65.7	0.19	0.02	
Kilauea Iki									
Iki 58	Hawaii OIB	50 yr	Pumice	SA		49.9	1.13	0.27	
Iki 22	Hawaii OIB	50 yr	Pumice	SA		46.7	0.94	0.22	
Iki3	Hawaii OIB	50 yr	Pumice	SA		47.2	2.19	0.52	
67-2-85.7	Hawaii OIB	50 yr	Basalt-andesite	SA		56.2	4.55	1.07	
67-3-6.8	Hawaii OIB	50 yr	Basalt	SA		44.6	0.71	0.17	
67-3-27.5	Hawaii OIB	50 yr	Basalt	SA		48.6	1.14	0.27	
67-3-75.2	Hawaii OIB	50 yr	Basalt	SA		50.1	2.04	0.48	[Mo] data from Greaney et al. (2017);
67-3-76.2	Hawaii OIB	50 yr	Basalt-andesite	LA		50.8	nd	-	Major element from Helz and Taggart (2010)
75-1-38.9	Hawaii OIB	50 yr	Basalt	SA		48.4	1.03	0.24	
75-1-121.5	Hawaii OIB	50 yr	Basalt-andesite	SA		50.0	1.33	0.31	
75-1-130.5	Hawaii OIB	50 yr	Basalt	LA		49.7	nd	–	
75-1-134.4/133.4	Hawaii OIB	50 yr	Olivine basalt	SA, LA	Yes	48.9	1.42	0.34	
79-1R1-170.9	Hawaii OIB	50 yr	Basalt-andesite	SA, LA	Yes	54.6	3.61	0.85	
79-3-150.4	Hawaii OIB	50 yr	Olivine basalt	SA, LA	Yes	48.4	1.03	0.24	
79-3-158.0	Hawaii OIB	50 yr	Basalt-andesite	SA, LA	Yes	52.4	2.30	0.54	
79-3-160.6/160.3	Hawaii OIB	50 yr	Olivine basalt	SA, LA	Yes	47.4	0.91	0.21	
79-3-171.9/172.8	Hawaii OIB	50 yr	Olivine basalt	SA, LA	Yes	46.6	0.85	0.20	
81-2-88.6	Hawaii OIB	50 yr	Basalt-andesite	SA, LA	Yes	57.1	4.70	1.11	
81-1-119.2	Hawaii OIB	50 yr	Basalt-andesite	SA		50.6	1.00	0.24	
81-1-169.9	Hawaii OIB	50 yr	Olivine basalt	SA		43.7	0.95	0.22	
81-1-210.0/209.8	Hawaii OIB	50 yr	Olivine basalt	SA, LA	Yes	44.9	0.57	0.14	
81-1-239.9	Hawaii OIB	50 yr	Olivine basalt	SA		44.2	0.56	0.13	
81-1-294.7	Hawaii OIB	50 yr	Olivine basalt	SA, LA	Yes	48.1	0.72	0.17	

Table 2
Secondary standards analyzed by laser ablation and standard addition. Concentrations are in μg/g. LA = Laser ablation-ICP-MS and SA = Standard addition whole rock-ICP-MS. BHVO-1 and AGV-2 were measured during the same analytical session as data reported in Greaney et al. (2017). Complete analytical methods can be found in the supplementary information.

secondary standard	Analysis	Mo (reported)	Mo 95 measured	2 s	Mo 97 measured	2 s	Mo 98 measured	2 s	n
BHVO-2g	LA	3.8	4.09	0.86	4.07	1.15	4.03	1.16	89
NIST 612	LA	37.4	43.6	16.2	40.4	14.0	44.1	7.89	8
JB sulfide	LA	2.55	2.44	0.30	2.45	0.69	2.44	0.20	8
BHVO-1	SA	1.1*	1.17	0.34	1.19	0.33	1.17	0.34	8
AGV-2	SA	1.93*	1.94	0.13	1.93	0.1	1.92	0.07	5

* Values from Gaschnig et al. (2015).

for analyses). The sulfides are volumetrically insignificant (<1 vol%) in all of the analyzed samples, and, for most samples, did not register in mineral modes determined by point counting (see the mass balance table in the supplement).

Molybdenum concentrations (designated as [Mo]) in accessory sulfides vary by approximately three orders of magnitude (0.01–9.2 μg/g). The maximum [Mo] is found in the Kilauea Iki lava-hosted sulfides (mean $[Mo]_{Kilauea\ sulfides} = 2.7$ μg/g, max = 9.2 μg/g) while the granite-hosted sulfides contain significantly less Mo than those from Kilauea Iki (mean $[Mo]_{granite\ sulfides} = 0.72$ μg/g, max = 8.0 μg/g, Fig. 2), but have similar concentrations to MORB-hosted sulfides (Patten et al., 2013). Molybdenite was not found as an accessory phase in any sample, but one grain of magnetite in a TTG from the Zimbabwe craton (ZB89-53) contains significant Mo (~1300 μg/g), along with Pb and other chalcophile elements. This suggests that a small nugget of MoS_2, or similar phase, may have been

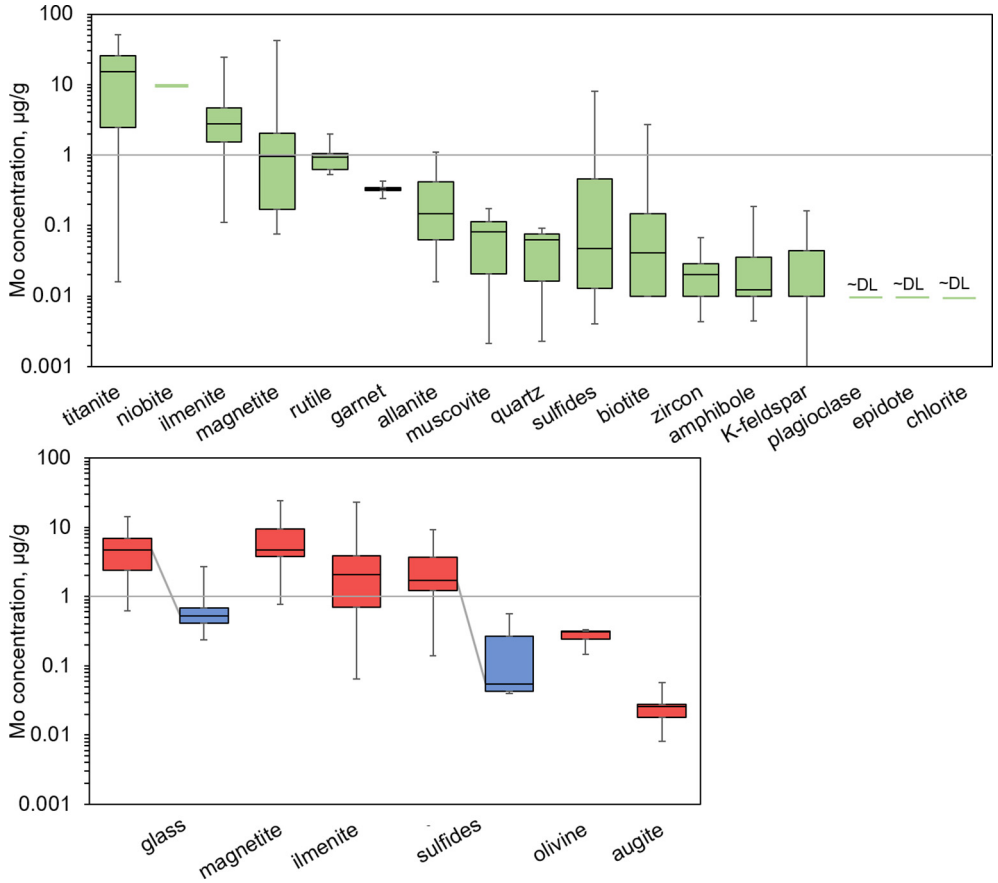

Fig. 2. Box and whisker plots of Mo abundances in all the minerals analyzed. Minerals are arranged by their median [Mo], with the boxes representing 1st and 3rd quartiles and whiskers representing min and max values measured. Upper plot: Granitic minerals from the Zimbabwe craton, Superior Province, and Phanerozoic granitic rocks. Plagioclase, epidote, and chlorite analyses were often below the detection limits. Lower plot: Minerals in basaltic to intermediate lavas from Kilauea Iki (red; data from Greaney et al. (2017)) and MORB (blue; glass data from Jenner and O'Neill (2012), sulfide data from Patten et al. (2013)). (For interpretation of the references to color in this figure legend, the reader is referred to the web version of this article.)

Table 3
Mean Mo concentrations in all minerals analyzed (including granitic rocks and basalts). 2σ represents two standard deviations of the mean of repeated analyses. Analyses of sulfides, quartz, amphibole, K-feldspar, zircon, plagioclase, and epidote were occasionally below the detection limits (~0.01 μg/g), so the detection limit of 0.01 μg/g was included in place of those analyses when calculating the mean concentration. Therefore, these data may be skewed to slightly higher values than actually present in the mineral.

	Titanite	Niobite	Magnetite	OIB Glass	Ilmenite	Sulfides	Rutile	Garnet	Allanite	Biotite
Mo (μg/g)	15.9	9.83	5.83	4.83	4.09	1.44	0.95	0.33	0.32	0.15
2σ	27.2	n/a	17.5	5.58	11.2	4.09	0.86	0.09	0.66	0.85
n	59	1	36	101	53	78	10	12	23	41
	Olivine	Muscovite	Quartz	Hornblende	K-feldspar	Augite	Zircon	Plagioclase	Epidote	Chlorite
Mo (μg/g)	0.10	0.08	0.05	0.04	0.03	0.02	0.02	≤0.01	≤0.01	≤0.01
2σ	0.15	0.13	0.06	0.10	0.08	0.02	0.03	0.03	0.01	n/a
n	5	9	25	36	24	5	21	37	19	1

embedded within or beneath the magnetite grain, but was not visible on the surface. This analysis was excluded from the magnetite data presented in Fig. 2 and Table 3.

4.1.2. Silicates and oxides

In addition to sulfides, quartz, K-feldspar, plagioclase, biotite, muscovite, hornblende, titanite, garnet, allanite, zircon, epidote, chlorite, olivine, clinopyroxene (augite), volcanic glass, magnetite, ilmenite, rutile, and the rare accessory phase columbite (also called niobite) were all analyzed for their Mo abundances (Table 3). The mean data presented in this table also include analyses that were below the LOD in plagioclase, K-feldspar, biotite, amphibole, muscovite, sulfides, epidote, and quartz. In these cases, the lower LOD commonly calculated for these analyses (0.01 μg/g=) was used to calculate the mean [Mo] value. Thus, the average concentrations for these phases should be considered maxima. Collectively, these data encompass nearly every major mineral found in common igneous rocks. Most phases were analyzed repeatedly across several rock types and localities except for columbite/niobite, which is confined to a single crystal in a Phanerozoic granite (07RMG52).

Molybdenum concentrations are presented in box and whisker plots in Fig. 2 with the phases arranged from highest to lowest [Mo], as established by the median [Mo] value. Molybdenum concentrations are considered to be significant if they are greater than 1 μg/g (average UCC [Mo] = 1.1 μg/g; Rudnick and Gao, 2014). Titanite consistently contains significant Mo, except for one sample from the Superior Province (WXP99-176), in which titanite contained between 0.01 and 0.5 μg/g. Metamorphic rutile replaced part of the titanite in that sample and may have preferentially incorporated Mo into its lattice, removing it from the titanite. Excluding this sample, [Mo] in titanite is commonly > 30 μg/g. Ilmenite and magnetite are the other two common phases that routinely contained ≥ 1 μg/g Mo in both granitic and basaltic samples. Rutile and columbite/niobite are less common upper crustal minerals, but they were found as primary igneous and secondary metamorphic assemblages in some samples and contain significant Mo. Volcanic glass was also found to be a significant host of Mo in the Kilauea samples where the average Mo_{glass} concentration is 4.8 μg/g. Glass data from ~600 MORB samples (Jenner and O'Neill, 2012) are shown for comparison, and have an average [Mo] of 0.62 μg/g, which is significantly lower than KI glass because MORB has lower whole-rock [Mo], and many of the KI lavas are more evolved than MORB. Most of the minerals analyzed do not contain abundant (>1 μg/g) Mo, including the most common minerals in granitic and basaltic rocks: quartz, feldspars, biotite, amphibole, olivine, and pyroxenes. Sulfides are found near the middle or right-hand side of each plot in Fig. 2, reflecting their generally low [Mo], relative to other minerals. Sulfide data from MORB (Patten et al., 2013) are shown for comparison to OIB sulfides on the plot of basaltic minerals.

4.1.3. Mass balance

Mineral modes were determined for the samples using a least-squares regression program, MINSQ (Herrmann and Berry, 2002). Select samples were also point counted to ensure accuracy of the MINSQ program (supplementary materials). The modal abundances are used together with the measured Mo concentrations to calculate the primary location of Mo (Fig. 3; mass balance provided in supplementary materials). Given their scarcity, sulfides were not registered in point counting exercises, so they were assigned modal abundances of 0.01–0.1%, which are likely to be overestimates in most samples. Nevertheless, in most samples the sulfide [Mo] contributes less than 3% of the whole-rock [Mo]. The maximum sulfide Mo contribution occurs in the Kilauea Iki volcanic rocks, where sulfides contain up to 6% of the total whole-rock [Mo]. By contrast, titaniferous phases are the dominant hosts of Mo in granitic rocks. Silicates can also contribute a significant portion of the total Mo budget (e.g., ~25% in one sample, Fig. 3), given their volumetric significance in granites. The calculated Mo distribution results in $[Mo]_{whole\ rock,\ calculated}$ that can be compared to measured whole rock data and $[Mo]_{whole\ rock,\ measured}$, to see if a mass balance is attained.

Given analytical uncertainties on the standard addition, laser ablation, and modal mineralogy measurements, we consider that mass balance is achieved if the calculated whole-rock abundance is within 20% of the measured whole-rock value. Of the ten granitic samples evaluated, mass balance is attained in only six. The remaining four are missing anywhere between 60 and 80% of the expected Mo abundance, based-on the whole-rock [Mo] measured by standard addition ICP-MS. All thin sections were carefully

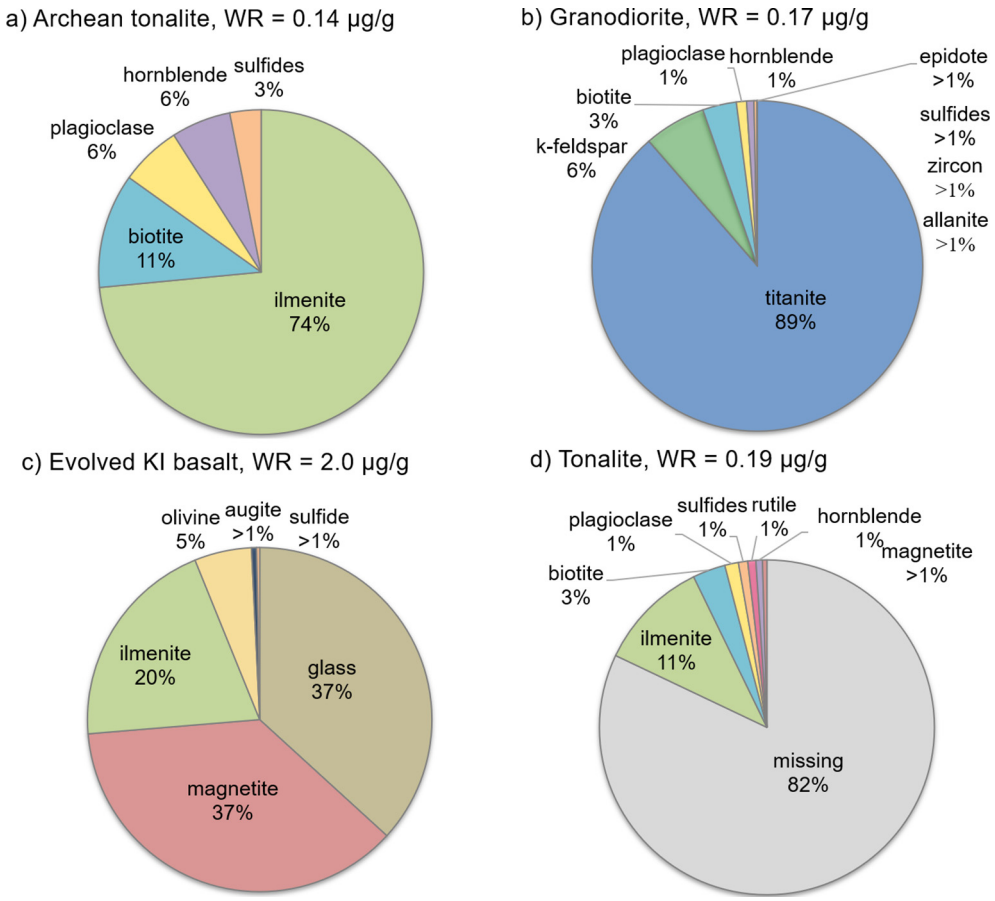

Fig. 3. Pie charts depicting the total Mo distribution in four samples selected to show variation in major host minerals. Mass balance is achieved in three of the samples depicted (a, b, c), but 82% of the whole-rock [Mo] is missing from sample d. Sample numbers: (A) WXP99-123, (B) AG1401, (C) KI67-3-76.2, (D) 10RMG005.

examined to ensure that no phase was missing from *in-situ* analysis. The incomplete mass balance is probably a real phenomenon, and is discussed further below.

4.2. Whole-rock data

Whole-rock [Mo] data are presented in Table 1 and a complete dataset, including major and trace elements (including Ga, Ge, Cd, In, Sn, Sb, W, Tl, and Bi), is presented in the online supplement. Almost all granitic rocks analyzed contain less than 1 µg/g Mo, except for three samples from Baffin Island. Several Kilauea Iki samples (data presented in Greaney et al., 2017) contain more than 1 µg/g because they are derived from an enriched mantle source and evolved further than most MORB, without Mo fractionation on a whole-rock scale.

4.2.1. Data representation

During mantle melting and igneous differentiation, Mo is expected to have similar partitioning behavior to the LREE, specifically Ce and Pr given their comparable ionic radii (Newsom and Palme, 1984). Therefore, Mo concentrations are plotted between these two elements on modified multi-element plots (Fig. 4) that have been normalized to the upper continental crust values of Rudnick and Gao (2014). In addition to LREE, Nb is included to indicate whether a sample has a Nb depletion (UCC normalized Nb/La < 1) that may be induced by Ti-oxide fractionation in the subducting slab or during differentiation. The majority of analyzed granitic rocks analyzed are depleted in Mo, relative to Ce and Pr. Only nine of the 45 samples show either a smooth LREE-Mo profile with no depletion, or are enriched in Mo. Given the normalized values for Ce and Pr, an expected Mo value (Mo^*) can be calculated as $([Ce]_n \times [Pr]_n)^{0.5}$ where "n" means normalized to the UCC value of Rudnick and Gao (2014). The percentage of Mo "missing" from a given sample can then be calculated as $100 \times (Mo^* - Mo_{meas})/Mo^*$. Between 20 and 90% (with a mean of 60%) of Mo is missing from the 36 samples that show Mo depletion, which equates to between 0.04 and 2.0 µg/g, depending on the sample. Details regarding the Mo^* calculation can be found in the supplement.

5. DISCUSSION

5.1. Mineralogical hosts of Mo

In igneous rocks, Mo is not primarily hosted in accessory sulfide minerals such as pyrite, pyrrhotite, and chalcopyrite. This is most probably due to the relatively

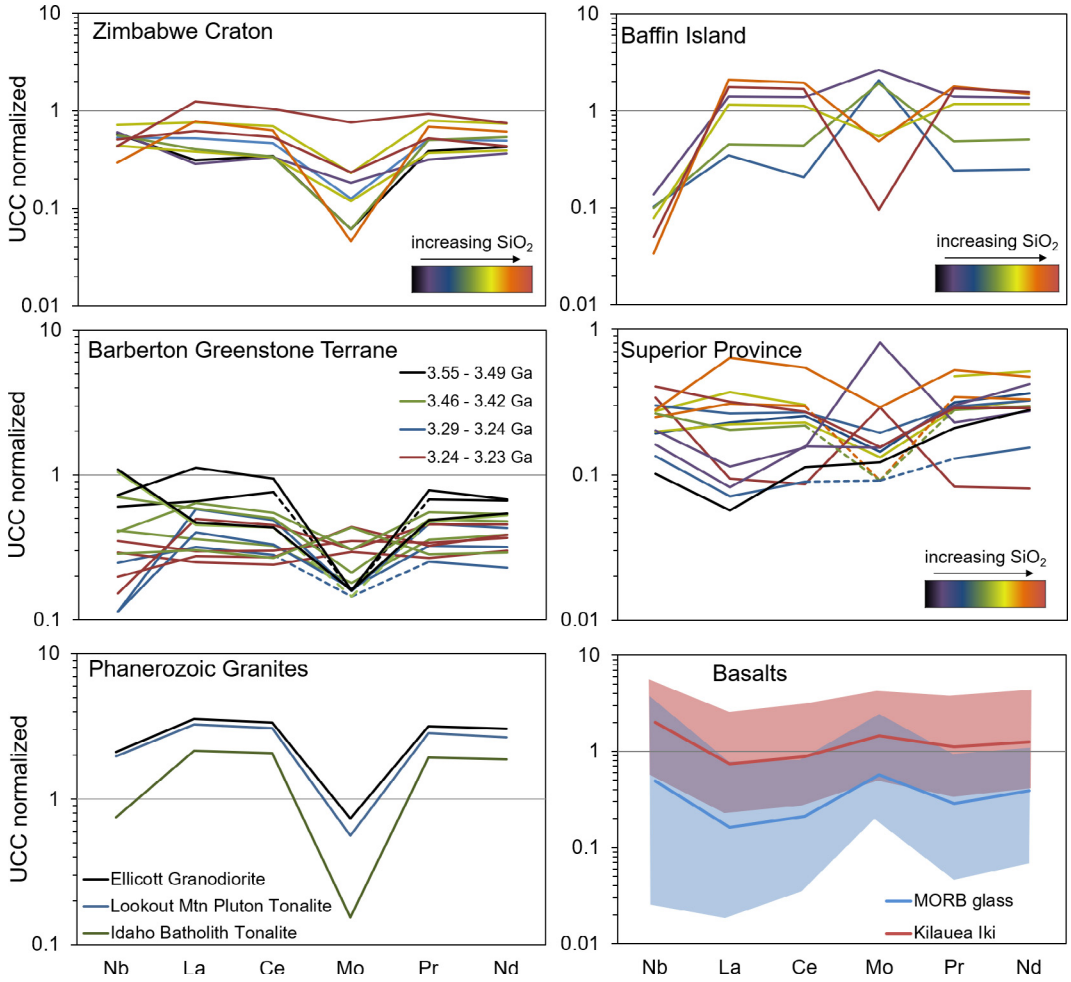

Fig. 4. UCC normalized spider plots showing Mo behavior relative to LREE in granitic suites (and their associated mafic enclaves/gabbros in the Superior and Baffin Island samples), and modern basalts. The differentiation suites from Zimbabwe, Baffin Island, and Superior Province are defined with a gradient color scale (note the SiO_2 range varies for each suite with black and purple representing mafic or intermediate samples). Dashed lines indicate that Mo was below the detection limit in that sample, so the detection limit is used as the [Mo] value (see Table 1). All data are normalized to the UCC (Rudnick and Gao, 2014). Baffin Island data, except for Mo abundances, come from Whalen et al. (2012). The Kilauea Iki field represents twenty samples (Greaney et al., 2017) and the MORB field represents ~600 glass samples from Jenner and O'Neill (2012), with the mean values for both datasets shown with a line. (For interpretation of the references to color in this figure legend, the reader is referred to the web version of this article.)

oxidized nature of magmas, in which Mo exists in its hexavalent state (O'Neill and Eggins, 2002), making the formation of MoS_2 rare. We conclude that Mo does not behave as a chalcophile element in primary magmatic settings, because it is not sufficiently reduced to be incorporated into a sulfide phase without the presence of abundant reduced sulfur. This contrasts with the behavior of Mo in the low-T epithermal systems that are commonly associated with pluton cooling, in which Mo^{6+} is reduced by H_2S in the exsolving fluids to form molybdenite (Hannah et al., 2007).

The most important Mo-bearing phases in the igneous rocks analyzed here are titanite ($[Mo]_{mean} = 15.9$ μg/g), magnetite ($[Mo]_{mean} = 5.83$ μg/g), ilmenite ($[Mo]_{mean} = 4.09$ μg/g), and glass ($[Mo]_{mean} = 4.83$ μg/g) (Fig. 2). Columbite ($FeNb_2O_6$) is also a significant Mo host in one sample from the Idaho batholith, but this is an uncommon mineral. As pointed out above, octahedrally coordinated Mo^{6+} has a similar ionic radius to octahedrally coordinated Ti^{4+} (73 and 74.5 pm, respectively; Shannon, 1976), which occurs in ilmenite, titanite, and rutile. Likewise, the ionic radius of tetrahedral Mo^{6+} is similar to tetrahedral Ti^{4+} (55 and 56 pm, respectively), which occurs in pseudobrookite (a common oxide mineral in the KI lavas) and other titaniferous spinel-group minerals. A coupled substitution with a divalent cation is needed to maintain electrical neutrality when hexavalent Mo replaces tetravalent Ti. This could be achieved by substitution of Fe^{2+} (ionic radius of 75 pm) into octahedrally coordinated sites. In pseudobrookite, for example, an additional mole PFU of Fe^{2+} replacing Fe^{3+} for each mole of Mo replacing Ti would satisfy charge balance.

Other minor Mo hosts include silicates such as garnet ($[Mo]_{mean} = 0.33$ μg/g) and biotite ($[Mo]_{mean} = 0.15$ μg/g). These results generally agree with those of Voegelin et al.

(2014) who found that biotite has the highest Mo abundance of any silicate analyzed in their study, which also included analyses of feldspars, hornblende, olivine, and pyroxenes ($[Mo]_{biotite,Voegelin} = 0.67$ μg/g), while feldspars contained less than 0.1 μg/g. Although these silicates have low Mo concentrations, their high volumetric abundances may contribute significantly to total crustal Mo abundances, as up to 25% of the total whole-rock Mo is attributed to silicates in one tonalite from the Superior Province (Fig. 3). Moreover, these phases are relatively easily altered, compared to the titaniferous phases, and will act as a source of Mo during continental weathering.

Molybdenite (MoS_2) was not observed in any of the samples analyzed here, but we propose that very small grains of MoS_2 could complete the mass balance in some samples. While it is relatively rare for it to occur as an accessory phase in granites, molybdenite, which contains 60% Mo by weight, is a highly-concentrated source of Mo in the crust, and occurs as a fairly common ore mineral that forms during epithermal processes associated with the emplacement of granitic plutons. Since it is so Mo-rich, an exceedingly small 'nugget' of MoS_2 (e.g., <0.0004 vol% of a thin section) could complete the mass balance in samples that show deficits between calculated and measured whole-rock [Mo]. While uncommon, MoS_2 inclusions in quartz have been documented in felsic igneous rocks (Audétat et al., 2011). The role of MoS_2 in the overall Mo budget of the crust, as well as the weathering properties of all Mo-bearing phases, are discussed further in Sections 5.2.2 and 5.2.3.

5.2. Mo behavior during magmatic differentiation

5.2.1. Mo depletion in granites

Depletion of Mo relative to Ce and Pr is observed in every granitic suite analyzed here, with most of the samples (36 out of 45) exhibiting Mo depletion. The depletion is evident whether the data are normalized to primitive mantle (McDonough and Sun, 1995) or UCC values (Rudnick and Gao, 2014), and is especially stark when compared to MORB and Kilauea Iki data, in which Mo has a similar or higher normalized abundance to the LREE (Fig. 4), as predicted by Newsom and Palme (1984). Additionally, recently published Mo data for granites from the Lachlan Fold Belt also show an UCC-normalized Mo depletion in the majority of samples for which published Ce data could be located (Yang et al., 2017, and references therein). The widespread depletion of Mo in granitic rocks may be due to the following two processes, which are not mutually exclusive: (a) Mo could be lost from an evolving magma to a fractionating titaniferous phase such as rutile or Fe-Ti oxides (Kuroda and Sandell, 1954; Fitton, 1995; Audétat et al., 2011), or (b) Mo could be lost to a magmatic vapor phase (MVP) exsolved from a cooling pluton (Candela and Holland, 1984; Audétat, 2010; Audétat et al., 2011). We also propose that S-type granites may show Mo depletion because their source (detrital sediments from oxidatively weathered sources) are depleted in Mo (per Gaschnig et al., 2014). However, with the exception of sample 07RMG52, the granitic rocks analyzed here are not proper S-type granites as determined by mineralogy and Aluminum Saturation Index, so this hypothesis does not apply to our data. The hypothesis that Mo is removed during crystal fractionation/accumulation in residual phases is evaluated by determining whether Mo depletion correlates with Nb depletion in the pluton suites, while MVP exsolution is evaluated by examining correlations between Mo and other fluid-soluble elements.

5.2.2. Hypothesis 1: loss of Mo due to partitioning into titaniferous phases

Within this first hypothesis, we propose two processes that may inhibit Mo from reaching the upper crust: (1) Mo-loss could be due to fractionation of titaniferous phases (e.g., ilmenite, magnetite, rutile, titanite) during igneous differentiation, and/or, (2) In arc settings, Mo could be retained in residual rutile in a subducting slab, like Nb. These are both likely explanations for the Mo depletion given the observed affinity that Mo has for rutile (Fitton, 1995; Zack et al., 2002) and other Ti-bearing phases like ilmenite and magnetite (Arnorsson and Oskarsson, 2006; Audétat, 2010; Greaney et al., 2017; this study), and they are not mutually exclusive. Titanite, a major host of Mo in most of the titanite-bearing samples analyzed here, could also potentially play a role in removing Mo and Nb as well (Marks et al., 2008), although it crystallizes relatively late in a cooling magma. A correlation between Mo/Ce and Nb/La is observed in several of the plutonic suites analyzed here (Fig. 5), suggesting that fractionation into Fe-Ti oxides during differentiation may remove these elements from an evolving magma. This process may sequester Mo and Nb in lower- or mid-crustal cumulates.

The Baffin Island Qikiqtarjuaq Plutonic Suite is an excellent example of differentiation from gabbro to granite. It exhibits a strong correlation between Mo/Ce and Nb/La ($R^2 = 0.92$, Fig. 5) suggesting that Mo and Nb share the same geochemical behavior as the magma evolved. All Baffin Island samples have an UCC-normalized Nb/La ratio < 1, suggesting that Nb was initially sequestered in rutile during subduction and mantle melting. The differentiation suite also displays a negative correlation between Nb and SiO_2 ($R^2 = 0.81$) and a negative correlation between Mo/Ce and SiO_2 ($R^2 = 0.75$) over a range from 50.3 to 72.3 wt% SiO_2, suggesting that both elements were removed by crystal fractionation, instead of behaving incompatibly (Fig. S2). In this plutonic suite, Nb was most likely held in residual rutile, and was then further sequestered in fractionating Fe-Ti oxides, along with Mo, during differentiation (Figs. 4 and 5). The Mo enrichments in the more mafic to intermediate samples may reflect an overabundance of these Mo-bearing minerals relative to the more evolved rocks. This decrease in Mo with differentiation contrasts with observations of Mo increase during differentiation at Hekla volcano, Iceland (Yang et al., 2015) and at Kilauea Iki, Hawaii (Greaney et al., 2017). There appears to be a correlation between Mo/Ce and Nb/La in the Superior Province samples as well (Fig. 5, $R^2 = 0.89$), although this strong correlation is achieved by ignoring an apparent outlier in the data. The Mashaba tonalities from the Zimbabwe Craton show a much weaker correlation between

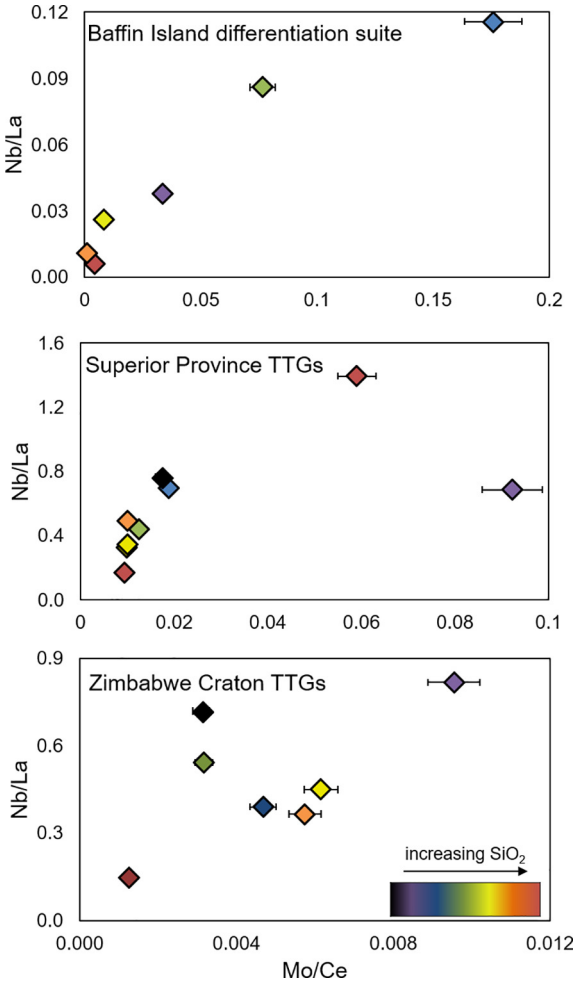

Fig. 5. Correlations between Mo/Ce and Nb/La in Archean and Proterozoic pluton suites. Samples are color coded based on SiO_2 content with red being the most felsic and purple/black being the least. The SiO_2 range varies between suites (see Table 1 and supplementary figures). The Zimbabwe data include only the Mashaba tonalite suite. Error bars represent 2σ external reproducibility, as determined by AGV measurements. (For interpretation of the references to color in this figure legend, the reader is referred to the web version of this article.)

Nb/La and Mo/Ce ($R^2 = 0.34$) and Ti/Gd and Mo/Ce ($R^2 = 0.42$). However, it should be noted that the degree of differentiation in the Zimbabwe tonalites is much less than that observed in other samples and that these samples have been interpreted to represent nearly pure partial melts of a basaltic source without significant fractional crystallization (Luais and Hawkesworth, 1994). Nevertheless, there is a strong correlation between Nb/Ta and SiO_2 in the Zimbabwe data, suggesting that a Ti-bearing phase (e.g., titanite) is being removed from this system during differentiation, but either is not taking Mo with it, or the fractionation signature is overprinted by another process (Fig. S3). We have insufficient data on Phanerozoic granites to draw conclusions about magmatic differentiation for those samples.

Molybdenum isotope studies also support the hypothesis that Mo is partitioned into fractionating Ti-bearing phases. Based on the data in Voegelin et al. (2014), Yang et al. (2017) propose that sequestration of Mo-bearing phases (they suggest biotite and hornblende) in the lower crust may explain the heavy δ^{98}Mo isotope signature observed in UCC rocks relative to basalts. Additionally, Wille et al. (2018) suggest that Mo isotopes may be fractionated during crystallization of amphibole or clinopyroxene in arc settings. Overall, a net isotope fractionation is observed between average UCC felsic rocks (~+0.15‰; Willbold and Elliott, 2017) and MORB (~0.0‰; Liang et al., 2017; Bezard et al., 2016) and OIB (~−0.14‰; Liang et al., 2017), suggesting that not only [Mo] but also Mo isotopes may be fractionated during igneous differentiation (Voegelin et al., 2014; Yang et al., 2017; Liang et al., 2017; Greber et al., 2015a, 2015b; Wille et al., 2018). By contrast, other studies show that Mo abundances and isotopes are not significantly fractionated by differentiation processes in intraplate and arc settings (Yang et al. 2015; Gaschnig et al., 2017a, 2017b).

Alternatively, many researchers have proposed that Mo abundances (Fitton, 1995) and isotopes may be fractionated during dehydration and partial melting of the subducting slab in arc settings (Willbold and Elliott, 2017; König et al., 2008). Specifically, Fitton (1995) observed that a coupled Mo and Nb depletion in arc magmas may represent sequestration of these elements in rutile in the subducting slab. Experimental work of Bali et al. (2012) found that at the Ni-NiO buffer, Mo is retained in rutile relative to slab fluids, adding credence to this hypothesis. While sulfides are not found to be major hosts of Mo in granites, Skora et al. (2017) demonstrated experimentally that sulfides and rutile can fractionate Mo during sediment/slab melting in a subduction zone, given sufficiently reducing conditions. This study did not measure Mo abundances in the sulfides or rutile, so partition coefficients are unknown. However, Zack et al. (2002) found that Mo is significantly enriched in rutile relative to sulfide minerals in eclogites and therefore conclude that sulfides contribute less than 5% of the total eclogite Mo budget. Audétat (2010) suggested that Mo may be sequestered in monosulfide solid solution (MSS) during partial melting (e.g., of slab/sediment) and igneous differentiation, given the measured $D^{MSS/melt} \sim 80$. However, a recent study of sulfide-saturated arc lavas found no Mo depletion after the onset of sulfide saturation during differentiation (Jenner, 2017). Instead, Mo is seemingly enriched in the resulting sulfide-depleted magmas. Further studies of Mo in magmatic differentiation suites and in subduction zones are needed to determine which exact phase/s, if any, is/are responsible for elemental and isotopic fractionation.

5.2.3. Hypothesis 2: Mo loss during fluid exsolution

As outlined by Audétat (2010) and Audétat et al. (2011), it is likely that Mo is lost from granites due to exsolution of aqueous magmatic fluids or vapor phases, because experimental studies show that Mo is partitioned into these phases (Candela and Holland, 1984; Zajacz et al., 2017). Partition coefficients ($D^{fluid/melt}$) vary due to the nature of different ligands (e.g., Cl, F) and salinity, but typically range from D = 1 to D = 20 (Zajacz et al., 2008). Molybde-

num loss during aqueous fluid exsolution would probably lead to the saturation of molybdenite (MoS_2) in epithermal veins surrounding the plutons and, on larger scales, formation of economically viable Mo porphyry deposits.

Some TTG suites show only a weak (e.g., Zimbabwe, Fig. 5) or no correlation (e.g., Barberton) between Mo and Nb or Mo and Ti, which suggests that fractionation of Mo by Ti- or Nb-bearing phases did not play a dominant role in the evolution of the Mo budgets of these magmas. Alternatively, fractionation may not be captured by the limited differentiation range in these TTGs. Nevertheless, these plutonic suites (except for one set of Barberton TTGs) still show significant Mo depletion. In the Zimbabwe suite, Mo is variably correlated with Cs ($R^2 = 0.84$), Sb ($R^2 = 0.73$), Pb ($R^2 = 0.56$), and As ($R^2 = 0.46$) (Fig. S4) all of which are moderately compatible in a low-salinity fluid phases (Zajacz et al., 2008), and these elements are known to be expelled from granitic plutons. However, several of these correlations hinge on a single data point (Fig. S4). There is no correlation between these fluid-mobile elements and incompatible, less-fluid mobile elements such as the LREE, implying that the fluid-mobile element concentrations are dominated by processes other than crystal-melt differentiation. Indeed, Mo is more strongly depleted relative to Ce in this suite of TTGs relative to other locales (lower Mo/Ce ratio in Fig. 5), so a vapor phase may have preferentially removed Mo from the Zimbabwe TTGs. In contrast to the Zimbabwe samples, no individual pluton suite displays convincing ($R^2 > 0.4$) multi-element correlations in the Barberton TTGs. Correlations between Mo and fluid-soluble elements are also not found for the Superior Province or Baffin Island samples. Thus, we suggest that different processes of Mo-loss from plutons (fluid exsolution v. crystal fractionation) may be acting on different plutonic suites, and these processes are not mutually exclusive.

If we explore the hypothetical end-member case in which the effects of crystal fractionation are assumed to be negligible, and Mo behaves as an incompatible element in all systems, then loss through fluid exsolution to form MoS_2 could account for all calculated Mo depletions. In this scenario, it can be inferred that approximately 60% (average Mo lost from a pluton – see supplement information on Mo^* calculation) of the Mo in un-weathered UCC granites is hosted in MoS_2. This is a maximum estimate, because it is likely that Mo loss from the magma during partial melting or crystal fractionation also occurs.

A simple calculation can be used to estimate the maximum amount of Mo released from plutons to form molybdenite. We start with the following parameters and assumptions: the continental crust covers 210×10^6 km^2 of the Earth's surface (Cawood et al., 2013) and, to a depth of 10 km, 40% of that area is granitic rock that initially contains 0.5 μg/g Mo (the average interpolated Mo abundance, Mo^*, of this study). Mean Mo loss from the granites in this study is 60%, and we initially assume that all Mo 'lost' is due to vapor-phase partitioning. With these assumptions, a maximum 10^{14} kg of Mo would have been released from UCC granitic plutons to form MoS_2. If we instead assume that granite only composes 20% of the upper 10 km of the crust, and only 10% of the Mo missing from a pluton is a result of MoS_2 formation, then approximately 10^{13} kg of Mo would have been released from UCC granitic rocks to form MoS_2. Thus, we conclude that a maximum of 10^{13}–10^{14} kg of Mo may be hosted in MoS_2 in the upper 10 km of the continental crust. The USGS has identified $\sim 10^{10}$ kg of Mo resources available for mining (rounding to the nearest order of magnitude) (USGS, 2009). This suggests that up to three to four orders of magnitude more Mo may lie inaccessible beneath the surface of the continental crust.

In summary, a combination of fractionation during differentiation and loss via vapor phase exsolution probably contributes to the total Mo loss recorded in granites. This would explain discrepancies between plutonic suites – among which some show strong Ti-mineral fractionation signatures and others do not – yet, nearly all of the samples studied here show depletions in total [Mo]. Further studies of magmatic suites formed by partial melting with Fe-Ti oxides in the residue, or differentiation involving fractionation of Fe-Ti oxides are needed to test these hypotheses.

5.3. Release of Mo during oxidative weathering of the UCC

Mo enrichments in black shales that form in euxinic (S-rich) ocean basins are first observed in the rock record at around 2.5 Ga and persist through the Phanerozoic, with a second period of increased Mo abundances beginning at the end of the Proterozoic (Anbar et al. 2007; Scott et al., 2008; Wille et al., 2007). These enrichments are interpreted to reflect changing atmospheric and oceanic oxidation states due to the GOE and the Neoproterozoic Oxidation Event. However, before Mo concentrations in black shales can be calibrated as a paleo-atmospheric oxybarometer, one must first know which O_2 sensitive mineral phases host Mo in the continental crust (Anbar et al., 2007). We have shown here that molybdenite, specifically, is the predominant sulfide host of Mo in the UCC, while other common magmatic sulfides and their subsolidus exsolution products (pyrite, chalcopyrite, etc.) do not contain significant Mo. Based on our findings, it is likely that Mo released from MoS_2 during oxidative weathering is the source of Mo enrichment observed in oceanic sediments since the GOE. Thus, experimentally-determined oxidation rates of MoS_2 at low pO_2 are needed to derive the pO_2 of the atmosphere during the GOE (e.g., Greber et al., 2015a, 2015b). While authigenic pyrite may host some Mo in sedimentary rocks (e.g., Gregory et al., 2017), Mo must first be removed from the primary igneous crust before it can be concentrated in these phases. If Mo was not released significantly from the igneous UCC prior to the GOE – which is likely given the lack of Mo depletion in pre-GOE diamictites (Gaschnig et al., 2014) – then authigenic sulfides were probably not a weatherable source of Mo from the continental crust at the time of the GOE.

Given the strength of the Ti-O bond, titaniferous phases are fairly resistant to weathering, so Mo will not be easily released from them, irrespective of pO_2. It is very likely that Mo remains in these minerals as the source rocks are weathered and the titaniferous minerals are incorporated into

sediments as detrital minerals. However, Mo is also highly enriched in volcanic glass – a phase that is susceptible to weathering in anoxic and oxic environments. Therefore, we propose that weathering of volcanic glass may have released Mo from the crust before the rise of atmospheric oxygen. As no Mo depletion is observed in the UCC before the GOE (Gaschnig et al., 2014), this process was probably not widespread on the continents. However, soluble Mo^{6+} may have been released into the pre-GOE oceans from submarine weathering of glassy basalt. This Mo might have been immediately reduced and sequestered if sufficient S, or another reductant, existed in the water column. Alternatively, if there was insufficient S in the water column to reduce Mo prior to the GOE (as suggested by Canfield (2005)), Mo might have remained in solution in pre-GOE oceans and is therefore not recorded in the marine rock record. This hypothesis has implications for the timing of the evolution of Mo-co-factored enzymes that fix nitrogen, as sufficient Mo must be present in the water column for it to be incorporated into these enzymes (Stüeken et al., 2015). However, this assumes that Mo is not immediately reduced once it is weathered out of volcanic glass, and that Mo is not hosted in secondary alteration phases. Both of these assumptions need to be tested with weathering models and analyses of Mo in altered basalts.

5.4. Molybdenum enrichments in rift-related magmas

The Barberton Terrane is composed of TTGs, greenstones (metamorphosed Archean basaltic rocks), and sedimentary units that were formed between 3.5 and 3.2 Ga. The samples studied here span 300 Myr in age and were formed during three to four distinct tectono-magmatic events at 3.5 Ga, 3.46 Ga, 3.29 Ga and 3.24 Ga (Clemens et al., 2006, Kröner et al., 1991). On the basis of field relationships and pluton geochemistry, Moyen et al. (2007) interpreted the terrane to have formed during collision of exotic blocks (3.55–3.42 Ga plutons) followed by a main orogenic event (3.25–3.21 Ga) during which the Badplaas pluton was emplaced. This was followed by post-orogenic collapse at 3.22–3.21 Ga, contemporaneous with emplacement of the Nelshoogte pluton in an extensional setting. The plutonic suites emplaced during accretion and the main orogenic stage exhibit Mo depletions relative to LREE (with the exception of one sample from the Stolzburg pluton, STZ), while the Nelshoogte (NLG) pluton, which is associated with post-orogenic collapse, is not depleted in Mo (Fig. 6). The concentrations of REE do not change significantly between the different suites, but the NLG plutonic suite is less enriched in LREE relative to HREE, and is slightly more magnesian. This observation that Mo is enriched in ~3.2 Ga rift-related magmas is similar to Mo-enrichments observed in rift-related magmas today.

Similarly, while many economic Mo deposits are associated with arc-derived, calc-alkaline magmas (Westra and Keith, 1981; Whalen et al., 2001), the highest-grade Mo-porphyry deposits are associated with rift settings (e.g., Climax-type deposits; Ludington and Plumlee, 2009), and alkaline magmas from continental rifts show significant Mo enrichments (Audétat, 2010; Audétat et al., 2011). The source of Mo in these rift-related magmas is unclear; both the lithospheric mantle and the continental crust have

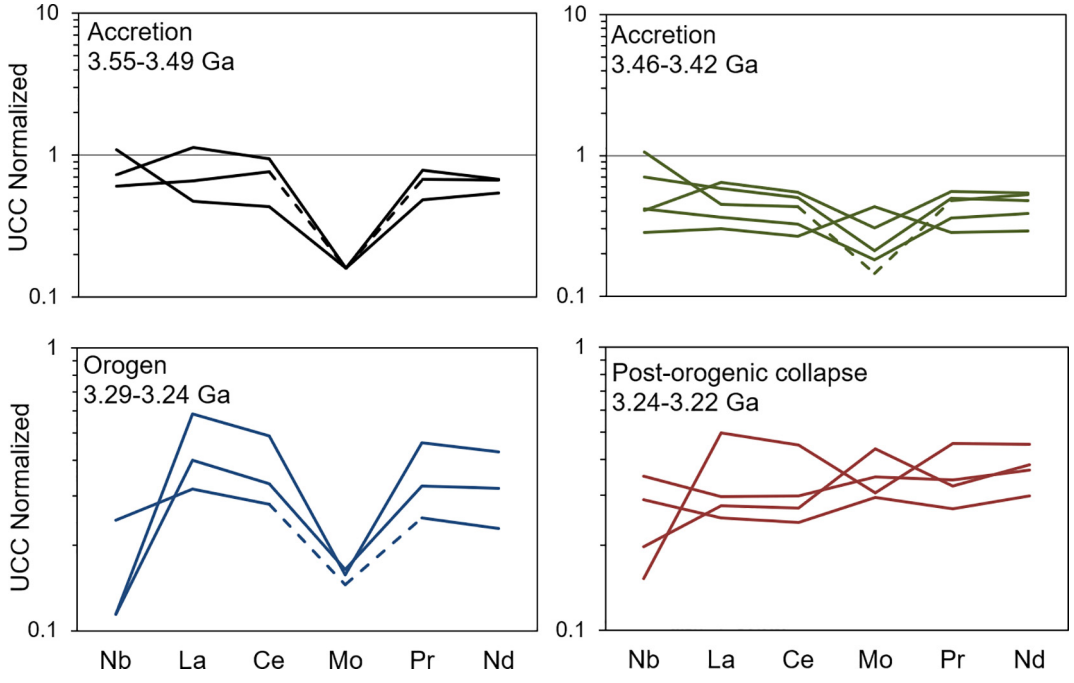

Fig. 6. UCC normalized spider plots for individual pluton suites in the Barberton Greenstone Belt representing different stages of accretion and post-orogenic collapse. Dashed lines indicate Mo was below the DL in the sample, so the DL is used instead of Mo concentration. Black = Steynsdorp; Green = Eerstehoek, Theespruit, Doornhoek, Stolzburg; Blue = Badplaas; Red = Nelshoogte. (For interpretation of the references to color in this figure legend, the reader is referred to the web version of this article.)

been suggested as sources. Sun et al. (2016) propose that assimilation of sedimentary rocks enriched in Mo (e.g., black shales) may be the source of Mo. Other researchers have suggested that the Mo may ultimately be sourced from Mo-enriched mantle melts that undergo fractional crystallization (Audétat, 2010; Pettke et al., 2010). Pettke et al. (2010) proposed that the lithospheric mantle may be re-enriched in Mo through subduction-related metasomatism, and that alkaline magmas may be generated from this Mo-rich reservoir during rifting events.

The observation that Mo is enriched in the ~3.2 Ga rift-related NLG pluton can be used to test these hypotheses. Significant Mo enrichments in black shales only occur after the onset of widespread oxidative weathering at ~2.4 Ga (Scott et al., 2008; Anbar et al., 2007). Thus, the hypothesis that rift magmas assimilate Mo-rich sediments, proposed by Sun et al. (2016) does not hold for these Archean magmas. There is evidence for subduction-related magmatism in the Barberton suite (Moyen et al., 2007; Furnes et al., 2012), which adds credence to the hypothesis that a subducting slab may have enriched the lithospheric mantle in Mo (Pettke et al., 2010). However, this hypothesis remains contentious because many authors argue that subduction zones mainly arose after 3.2 Ga (e.g., Condie and Kröner, 2008; Tang et al., 2016, and references therein).

In the Barberton samples, Mo correlates with Ni (Fig. 7a) and Cr (Fig. 7b). Additionally, the overall Mo enrichment of the NLG pluton relative to LREE resembles that of MORB and Hawaiian lavas (Fig. 4), suggesting a mafic, *i.e.,* mantle, origin for the Mo. Lithospheric mantle-derived Mo is a something of a paradox because the lithospheric mantle is refractory and should be depleted in incompatible Mo. This paradox could be resolved if the lithospheric mantle were metasomatized with fluids derived from a subducting slab, and then partially melted during a subsequent rifting event (Pettke et al., 2010). Alternatively, it is possible that the Mo enrichments may be derived from partial melting of Mo-rich cumulates (e.g., Fe-Ti oxides and rutile bearing rocks such as amphibolites and eclogites) during continental rifting. In this scenario, lower crustal rocks may contain the missing Mo recorded in granitic suites and explain the origin of the Mo enrichment in various rift-related magmatic suites. This hypothesis implies that sequestration of Mo in Fe-Ti oxides in lower crustal cumulates must be significant, and further analyses of Mo abundances in such rocks are needed to evaluate this idea.

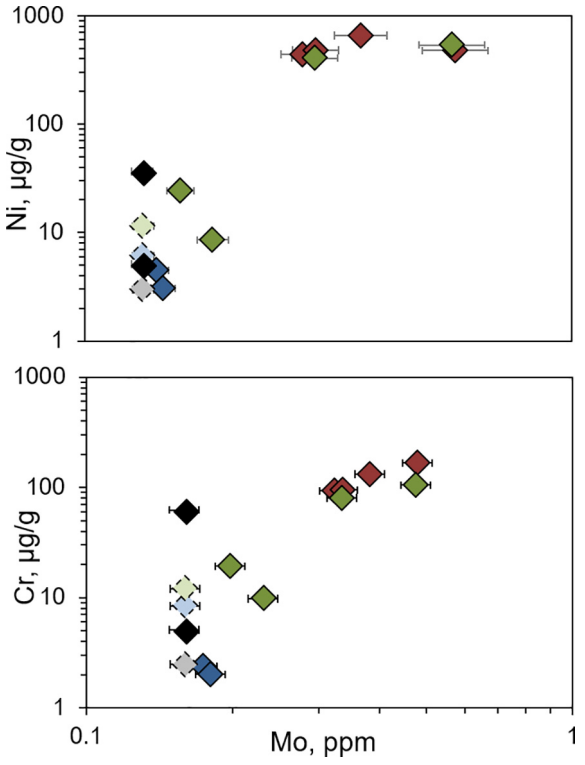

Fig. 7. Correlations between (A) Mo and Ni and (B) Mo and Cr in the Barberton TTGs. Color scheme is the same as in Fig. 6; dashed symbols represent samples that contain less Mo than the detection limit (0.16 µg/g). Error bars represent 2σ.

6. CONCLUSIONS

- In 'common' UCC granitic rocks, Mo is hosted primarily in weathering-resistant, titaniferous phases such as titanite, ilmenite, and magnetite, while in basaltic to andesitic volcanic rocks, Mo is predominately hosted in ilmenite, magnetite, and interstitial glass. Molybdenum mass balance based on in situ analyses of Mo in silicates and oxides cannot be completed in a few granitic samples, suggesting nuggets of MoS_2 may be a significant Mo host in some felsic plutonic rocks.
- Silicates (e.g., quartz, biotite, and amphibole) generally contain less than 0.2 µg/g Mo, but may be volumetrically significant hosts, contributing up to 25% of the whole-rock Mo in one granitic rock analyzed here.
- Common accessory phase sulfides (e.g., pyrite, chalcopyrite, immiscible sulfide blebs) are not significant hosts of Mo in granitic or basaltic rocks.
- Nearly all analyzed granitic rocks are depleted in Mo (by 20–90%, mean = 60%), relative to Ce and Pr. This may reflect MoS_2 precipitation from fugitive magmatic vapor phases or loss of Mo to fractionating Ti- and Nb-bearing phases during slab melting or magmatic differentiation. Some plutonic suites show correlations between Mo and Nb, suggesting loss of Mo due to fractionation of Fe-Ti oxides or other titaniferous phases. Other plutonic suites show correlations between Mo and fluid-soluble elements (e.g., Cs, Pb, As, etc.), potentially pointing to Mo loss in an aqueous magmatic vapor phase.
- If all Mo lost from granitic rocks is attributed to aqueous fluid exsolution and subsequent MoS_2 precipitation, then, on average, 60% of the Mo budget in a pluton would have to be concentrated in distal, epithermal veins that crystallized MoS_2. This is most likely an overestimate as it represents the endmember scenario where all Mo is lost through vapor-phase fractionation.
- The ~3.2 Ga rift-related Nelshoogte pluton from the Barberton Greenstone Belt is the only group of samples studied here that do not show a systematic Mo depletion. This is similar to observations of Mo-enrichments

in modern rift-related magmas. These data can be used to rule out the hypothesis that Mo enrichments in rift-related magmas are derived from melting of Mo-rich sediments like black shales, because Mo was not enriched in black shales prior to the GOE at ~2.4 Ga. If subduction was occurring at this time, subduction-related metasomatism of the lithospheric mantle could be the source of the enrichment in Mo in these rift-related magmas (Pettke et al., 2010). Alternatively, mantle melts generated during rifting may have assimilated Mo-rich residues in the lower crust or upper mantle to create these Mo enrichments in rift-related magmas. This would imply that significant Mo is removed from evolving magmas in Fe-Ti oxides. Further analyses of Mo in differentiated suites and lower crustal cumulates are needed to test this hypothesis.

- The processes of Mo-loss through fluid/vapor-phase partitioning or fractionation of titaniferous phases are likely not mutually exclusive. Here we present arguments for the two end-member scenarios but emphasize that further research is needed to determine the proportion of Mo-loss by these two processes.

ACKNOWLEDGEMENTS

We thank Aleisha Johnson, George Helz, Gary Stevens, and Scott Wipperfurth for valuable discussions, Richard Ash, Phil Piccoli, and Andrew Kylander-Clark for analytical assistance, and Steve Romaniello for assistance in reproducing the whole-rock data in the ASU Keck Lab for Biogeochemistry. We also thank the three reviewers (Thomas Ulrich, and two anonymous reviewers) for their suggestions that helped us to improve the paper. The work was supported by a National Science Foundation grant EAR 133810 (A. Anbar, PI; R.L. Rudnick, co-I), EAR 1757313, and the University of Maryland.

APPENDIX A. SUPPLEMENTARY MATERIAL

Supplementary data associated with this article can be found, in the online version, at https://doi.org/10.1016/j.gca.2018.06.039.

REFERENCES

Anbar A. D., Duan Y., Lyons T. W., Arnold G. L., Kendall B., Creaser R. A., Kaufman A. J., Gordon G. W., Scott C., Garvin J. and Buick R. (2007) A whiff of oxygen before the great oxidation event? *Science* **317**, 1903–1906.

Arnold G. L., Anbar A. D., Barling J. and Lyons T. W. (2004) Molybdenum isotope evidence for widespread anoxia in mid-proterozoic oceans. *Science* **304**, 87–90.

Arnorsson S. and Oskarsson N. (2006) Molybdenum and tungsten in volcanic rocks and in surface and <100 °C ground waters in Iceland. *Geochim. Cosmochim. Acta* **71**, 284–304.

Audétat A. (2010) Source and evolution of molybdenum in the porphyry Mo (-Nb) deposit at Cave Peak, Texas. *J. Petrol.* **51** (8), 1739–1760.

Audétat A., Dolejs D. and Lowenstern J. B. (2011) Molybdenite saturation in silicic magmas: occurrence and petrological implications. *J. Petrol.* **52**(5), 891–904.

Bali E., Keppler H. and Audetat A. (2012) The mobility of W and Mo in subduction zone fluids and the Mo-W-Th-U systematics of island arc magmas. *Earth Planet Sci Lett.* **351–352**, 195–207.

Bezard R., Fischer-Godde M., Hamelin C., Brennecka G. A. and Kleine T. (2016) The effects of magmatic processes and crustal recycling on the molybdenum stable isotopic composition of Mid-Ocean Ridge Basalts. *Earth Planet Sci Lett.* **453**, 171–181.

Candela P. A. and Holland H. D. (1984) The partitioning of copper and molybdenum between silicate melts and aqueous fluids. *Geochim. Cosmochim. Acta* **48**, 373–380.

Canfield D. E. (2005) The early history of atmospheric oxygen: homage to Robert M. Garrels. *Annu. Rev. Earth Planet. Sci* **33**, 1–36.

Cawood P. A., Hawkesworth C. J. and Dhuima B. (2013) The continental record and the generation of the continental crust. *GSA Bull.* **125**, 14–32.

Clemens J. D., Yearron L. M. and Stevens G. (2006) Barberton (South Africa) TTG magmas: geochemical and experimental constraints on source-rock petrology, pressure of formation and tectonic setting. *Precambrian Res.* **151**, 53–78.

Condie K. C. (1993) Chemical composition and evolution of the upper continental crust: Contrasting results from surface samples and shales. *Chem. Geol.* **104**, 1–37.

Condie and Kröner (2008) When did plate tectonics begin? Evidence from the geologic record. *GSA Spec. Pap.* **440**, 281–294.

Dahl T. W., Canfield D. E., Rosing M. T., Frei R. E., Gordon G. W., Knoll A. H. and Anbar A. D. (2011) Molybdenum evidence for expansive sulfidic water masses in ~750 Ma oceans. *Earth Planet Sci Lett.* **311**, 264–274.

Dhuime B., Wuestefeld A. and Hawkesworth C. J. (2015) Emergence of modern continental crust about 3 billion years ago. *Nat. Geosci.* **8**, 552–555.

Erickson B. E. and Helz G. R. (2000) Molybdenum(VI) speciation in sulfidic waters: stability and lability of thiomolybdates. *Geochim. Cosmochim. Acta* **64**, 1149–1158.

Farquhar J., Bao H. and Thiemens M. (2000) Atmospheric influence of Earth's earliest sulfur cycle. *Nature* **289**, 756–758.

Fitton J. G. (1995) Coupled molybdenum and niobium depletion in continental basalts. *Earth Planet Sci Lett.* **136**, 715–721.

Freymuth H., Vils F., Willbold M., Taylor R. and Elliot T. (2015) Molybdenum mobility and isotopic fractionation during subduction at the Mariana arc. *Earth Planet Sci Lett.* **432**, 176–186.

Furnes H., Robins B. and De Wit M. J. (2012) Geochemistry and petrology of lavas in the upper Onverwacht suite, Barberton Mountain Land, South Africa. *S. Af. J. Geol.* **115**, 171–210.

Gaschnig R. M., Vervoort J. D., Lewis R. S. and Tikoff B. (2011) Isotopic evolution of the Idaho Batholith and Challis Intrusive Province, Northern US Cordillera. *J. Petrol.* **52**(12), 2397–2429.

Gaschnig R. M., Rudnick R. L., McDonough W. F., Kaufman A. J., Hu Z. and Gao S. (2014) – Onset of oxidative weathering of continents recorded in the geochemistry of ancient glacial diamictites. *Earth Planet Sci Lett.* **408**, 87–99.

Gaschnig R. M., Rudnick R. L. and McDonough W. (2015) Standard addition ICP-MS characterization of selected chalcophile and siderophile elements (Ga, Ge, Mo, Ag, Cd, In, Sn, Sb, W, Tl, and Bi) in USGS whole-rock standard reference materials. *Geostan. Geoanal. Res.* **39**, 371–379.

Gaschnig R. M., Rudnick R. L., McDonough W. F., Kaufman A. J., Valley J. W., Gao S. and Beck M. (2016) Compositional evolution of the upper continental crust through time, as constrained by ancient glacial diamictites. *Geochim. Cosmochim. Acta* **186**, 316–343.

Gaschnig R. M., Macho A. S., Fayon A., Schmitz M., Ware B. D., Vervoort J. D., Kelso P., LaMaskin T. A., Kahn T. J. and Tikoff B. (2017a) Intrusive and depositional constraints on the

Cretaceous tectonic history of the southern Blue Mountains, eastern Oregon. *Lithosphere* **9**, 265–282.

Gaschnig R. M., Reinhard C. T., Planavsky N. J., Wang X., Asael D. and Chauvel C. (2017b) The molybdenum isotope system as a tracer of slab input in subduction zones: an example from Martinique, Lesser Antilles Arc. *Geochem. Geophys. Geosyst.* **18**, 4674–4689.

Goldschmidt V. M. (1937) *The Principles of Distribution of Chemical Elements in Minerals and Rocks*. Chemical Society, Hugo Müller Lecture.

Greaney A. T., Rudnick R. L., Helz R. T., Gaschnig R. M., Piccoli P. M. and Ash R. D. (2017) The behavior of chalcophile elements during magmatic differentiation as observed in Kilauea Iki Lava Lake, Hawaii. *Geochim. Cosmochim. Acta* **210**, 71–96.

Greber N. D., Mader U. and Nagler T. F. (2015a) Experimental dissolution of molybdenum-sulphides at low oxygen concentrations: a first order approximation of late Archean atmospheric conditions. *Earth Space Sci.* **5**, 173–180.

Greber N. D., Puchtel I. S., Nagler T. F. and Mezger K. (2015b) Komatiites constrain molybdenum isotope composition of the Earth's mantle. *Earth Planet. Sci. Lett* **421**, 129–138.

Gregory D. D., Lyons T. W., Large R. L., Jiang G., Stepanov A. S., Diamond C. W., Figueroa M. C. and Olin P. (2017) Whole rock and discrete pyrite geochemistry as complementary tracers of ancient ocean chemistry: an example from the Neoproterozoic Doushantuo Formation, China. *Geochim. Cosmochim. Acta* **216**, 201–222.

Hannah J. L., Stein H. J., Wieser M. E., de Laeter J. R. and Varner M. D. (2007) Molybdenum isotope variations in molybdenite: vapor transport and Rayleigh fractionation of Mo. *Geology* **35**, 703–706.

Hawkesworth C. J., Bickle M. J., Gledhill A. R., Wilson J. F. and Orpen J. L. (1979) A 2.9 Ga event in the Rhodesian Archaean. *Earth Planet Sci Lett* **43**, 285–297.

Helz Rosalind Tuthill, and Taggart Joseph E., Jr. (2010). Whole-Rock Analyses of Core Samples from the 1988 Drilling of Kilauea Iki Lava Lake, Hawaii. USGS Open File Report.

Helz G. R., Miller C. V., Charnock J. M., Mosselmans J. F. W., Pattrick R. A. D., Garner C. D. and Vaughan D. J. (1996) Mechanism of molybdenum removal from the sea and its concentration in black shales: EXAFS evidence. *Geochim. Cosmochim. Acta* **60**(19), 3631–3642.

Herrmann W. and Berry R. F. (2002) MINSQ – a least squares spreadsheet method for calculating mineral proportions from whole rock major element analyses. *Geochem.: Explor. Environ. Anal.* **2**, 361–368.

Holzheid A., Borisov A. and Palme H. (1994) The effect of oxygen fugacity and temperature on solubilities of nickel, cobalt, and molybdenum in silicate melts. *Geochim. Cosmochim. Acta* **58**(8), 1975–1981.

Jenner F. E. (2017) Cumulate causes for the low contents of sulfide-loving elements in the continental crust. *Nat. Geosci.* **10**, 524–529.

Jenner F. E. and O'Neill H. S. C. (2012) Analysis of 60 elements in 616 ocean floor basaltic glasses. *Geochem. Geophys. Geosyst.* **13** (1), 1–11.

Kasting J. F. (2014) Modeling the Archean atmosphere and climate. In Treatise on Geochemistry, second ed.pp. 157–173.

Kröner A., Byerly G. R. and Lowe D. R. (1991) Chronology of early Archaean granite-greenstone evolution in the Barberton Mountainland, South Africa, based on precise dating by single zircon evaporation. *Earth Planet Sci Lett.* **103**, 41–54.

König S., Wille M., Voegelin A. and Schoenberg R. (2008) Molybdenum isotope systematics in subduction zones. *Earth Planet Sci Lett.* **447**, 95–102.

Kuroda P. K. and Sandell E. B. (1954) Geochemistry of molybdenum. *Geochim. Cosmochim. Acta* **6**, 35–63.

Liang Y., Halliday A. N., Siebert C., Fitton J. G., Burton K. W., Wang K. and Harvey J. (2017) Molybdenum isotope fractionation in the mantle. *Geochim. Cosmochim. Acta* **199**, 91–111.

Lodders K. and Palme H. (1991) On the chalcophile character of molybdenum; determination of sulfide/silicate partition coefficients of Mo and W. *Earth Planet Sci Lett.* **103**, 311–324.

Luais B. and Hawkesworth C. J. (1994) The generation of continental crust: an integrated study of crust-forming processes in the Archaean of Zimbabwe. *J. Petrol.* **35**, 43–93.

Luais B. and Hawkesworth C. J. (2002) Pb isotope variations in the Archean and possible links to the sources of certain Mesozoic-Recent basalts. In *The Early Earth: Physical, Chemical and Biological Development*, vol. 199 (eds. C. M. R. Fowler, C. J. Ebinger and C. J. Hawkesworth). Geological Society, London, Special Publications, pp. 105–124.

Lyons T. W., Reinhard C. T. and Planavsky N. J. (2014) The rise of oxygen in Earth's early ocean and atmosphere. *Nature* **506**, 307–1215.

Ludington S., and Plumlee G. S. (2009) Climax-type porphyry molybdenum deposits: U.S. Geological Survey Open-File Report 2009–1215.pp. 1–16.

Marks M. A., Coulson I. M., Schilling J., Jacob D. E., Schmitt A. K. and Markl G. (2008) The effect of titanite and other HFSE-rich mineral (Ti-bearing andradite, zircon, eudialyte) fractionation on the geochemical evolution of silicate melts. *Chem. Geol.* **257**, 153–172.

McDonough W. F. and Sun S. S. (1995) The composition of the Earth. *Chem. Geol.* **120**, 223–253.

Miller C. A., Peuker-Ehrenbrink B., Walker B. D. and Marcantonio F. (2011) Re-assessing the surface cycling of molybdenum and rhenium. *Geochim. Cosmochim. Acta* **675**, 7146–7179.

Moyen J. F., Stevens G., Kisters A. F. M. and Belcher R. W. (2007) TTG plutons of the Barberton Granitoid-Greenstone Terrain, South Africa. *Precamb. Ophiolites Relat. Rocks Dev. Precamb. Geol.* **15**, 1–62.

Newsom H. E. and Palme H. (1984) The depletion of siderophile element sin the Earth's mantle: new evidence from molybdenum and tungsten. *Earth Planet Sci Lett.* **69**, 354–364.

O'Neill H. S. C. and Eggins S. M. (2002) The effect of melt composition on trace element partitioning; and experimental investigation of the activity coefficients of FeO, NiO, CoO, MoO_2 and MoO_3 in silicate melts. *Chem. Geol.* **186**, 151–181.

Palme H. and O'Neill H. S. C. (2004) Cosmochemical estimates of mantle composition. In Treatise on Geochemistry, first ed.pp. 1–38.

Paton C., Hellstrom J., Paul B., Woodhead J. and Hergt J. (2011) Iolite: Freeware for the visualisation and processing of mass spectrometric data. *J. Anal. Atom. Spectrom.* **26**, 2508–2518.

Patten C., Barnes S., Mathez E. A. and Jenner F. E. (2013) Partition coefficients of chalcophile elements between sulfide and silicate melts and the early crystallization history of sulfide liquid: LA-ICP-MS analysis of MORB sulfide droplets. *Chem. Geol.* **358**, 170–188.

Pettke T., Oberli F. and Heinrich C. A. (2010) The magma and metal source of giant porphyry-type ore deposits, based on lead isotope microanalysis of individual fluid inclusions. *Earth Planet Sci Lett.* **296**, 267–277.

Rayner N. M., Sanborn-Barrie S., Young M. D. and Whalen J. B. (2012) U-Pb ages of Archean basement and Paleoproterozoic plutonic rocks, southern Cumberland Peninsula, eastern Baffin Island, Nunavut. *Geol. Surv. Canada, Curr. Res. 2012-8*, 1–24.

Rudnick R. L. and Gao S. (2014) Composition of the continental crust. In Treatise on Geochemistry, second ed.pp. 1–45.

Scott C., Lyons T. W., Bekker A., Shen Y., Poulton S. W., Chu X. and Anbar A. D. (2008) Tracing the stepwise oxygenation of the Proterozoic ocean. *Nature* **452**, 456–459.

Shannon R. D. (1976) Revised effective ionic radii and systematic studies of interatomic distances in halides and chalcogenides. *Acta Cryst* **32**, 751–767.

Siebert C., Nägler T. F., von Blanckenburg R. and Kramers J. D. (2003) Molybdenum isotope records as a potential new proxy for paleoceanography. *Earth Planet Sci Lett.* **211**, 159–171.

Skora S., Freymuth H., Blundy J., Elliott T. and Guillong M. (2017) An experimental study of the behaviour of cerium/molybdenum ratios during subduction: implications for tracing the slab component in the Lesser Antilles and Mariana Arc. *Geochim. Cosmochim. Acta* **212**, 135–155.

Stein H. J. (1985) A lead, strontium, and sulfur isotope study of Laramide-Tertiary intrusions and mineralization in the Colorado Mineral Belt with emphasis on Climax-type porphyry molybdenum systems plus a summary of other newly acquired isotopic and rare earth element data [Ph.D. thesis]. University of North Carolina, Chapel Hill.p. 493.

Sun W., Li C., Hao X., Ling M., Ireland T., Ding X. and Fan W. (2016) Oceanic anoxic events, subduction style, and molybdenum mineralization. *Solid Earth Sci.* **1**, 64–73.

Stüeken E. E., Buick R., Guy B. M. and Koehler M. C. (2015) Isotopic evidence for biological nitrogen fixation by molybdenum-nitrogenase from 3.2 Gyr. *Nature* **520**, 666–669.

Tang M., Chen K. and Rudnick R. L. (2016) Archean upper crust transition from mafic to felsic marks the onset of plate tectonics. *Science* **351**, 372–375.

Taylor S. R. and McLennan S. (1985) *The Continental Crust: Its Composition and Evolution*. Blackwell, Malden, MA.

Turekian K. K. and Bertine K. K. (1971) Deposition of molybdenum and uranium along the major ocean ridge systems. *Nature* **229**, 250–251.

United States Geological Survey (2009) Mineral commodity summaries 2009: U.S. Geological Survey.p. 195.

Voegelin A. R., Pettke T., Greber N. D., von Niederhäusern B. and Nägler T. F. (2014) Magma differentiation fractionates Mo isotope ratios: evidence from the Kos Plateau Tuff (Aegean Arc). *Lithos* **190–191**, 440–448.

Walker R. J. (2016) Siderophile elements in tracing planetary formation and evolution. *Geochem. Perspect.* **5**(1), 1–143.

Westra G. and Keith S. B. (1981) Classification and genesis of stockwork molybdenum deposits. *Econ. Geol.* **76**, 844–873.

Whalen J. B., Anderson R. G., Struik L. C. and Villeneuve M. E. (2001) Geochemistry and Nd isotopes of the François Lake plutonic suite, Endako batholith: host and progenitor to the Endako molybdenum camp, central British Columbia. *Can. J. Earth Sci.* **38**, 603–618.

Whalen J. B., Percival J. A., McNicoll V. J. and Longstaffe F. J. (2002) A mainly crustal origin for tonalitic granitoid rocks, Superior Province, Canada: implications for Late Archean tectonomagmatic processes. *J. Petrol.* **43**(8), 1551–1570.

Whalen J. B., Percival J. A., McNicoll V. J. and Longstaffe F. J. (2003) Intra-oceanic production of continental crust in a Th-depleted ca. 3.0 Ga arc complex, western Superior Province, Canada. *Contrib. Mineral. Petrol.* **146**, 78–99.

Whalen J. B., Wodicka N., Taylor B. E. and Jackson G. D. (2010) Cumberland batholith, Trans-Hudson Orogen, Canada: petrogenesis and Implications for Paleoproterozoic crustal and orogenic processes. *Lithos* **117**, 99–118.

Whalen J. B., Sanborn-Barrie M., Young M. (2012) Geochemical data from Archean and Paleoproterozoic plutonic and volcanic rocks of Cumberland Peninsula, eastern Baffin Island, Nunavut, Geol. Survey Canada Open File 6933.

Willbold M. and Elliot T. (2017) Molybdenum isotope variations in magmatic rocks. *Chem. Geol.* **449**, 253–268.

Willbold M., Hibbert K., Lai Y.-J., Freymuth H., Hin R. C., Coath C., Vils F. and Elliott T. (2016) High-precision mass-dependent molybdenum isotope variations in magmatic rocks determined by double-spike MC-ICP-MS. *Geostan. Geoanal. Res.* **40**, 389–403.

Wille M., Kramers J. D., Nagler T. F., Beukes N. J., Schroder S., Meisel Th., Lacassie J. P. and Voegelin A. R. (2007) Evidence for a gradual rise of oxygen between 2.6 and 2.5 Ga from Mo isotopes and Re-PGE signatures in shales. *Geochim. Cosmochim. Acta* **71**, 2417–2435.

Wille M., Nebel O., Pettke T., Vroon P. Z., Konig S. and Schoenberg R. (2018) Molybdenum isotope variations in calc-alkaline lavas from the Banda arc, Indonesia: assessing the effect of crystal fractionation in creating isotopically heavy continental crust. *Chem. Geol.* **485**, 1–13.

Williamson M. A. and Rimstidt J. D. (1994) The kinetics and electrochemical rate-determining step of aqueous pyrite oxidation. *Geochim. Cosmochim. Acta* **58**, 5443–5454.

Yang J., Siebert C., Barling J., Savage P., Liang Y. and Halliday A. (2015) Absence of molybdenum isotope fractionation during magmatic differentiation at Hekla volcano, Iceland. *Geochim. Cosmochim. Acta* **162**, 126–136.

Yang J., Barling J., Siebert C., Fietzke J., Stephens E. and Halliday A. N. (2017) The molybdenum isotopic compositions of I-, S-, and A-type granitic suites. *Geochim. Cosmochim. Acta* **205**, 168–186.

Zack T., Kronz A., Foley S. F. and Rivers T. (2002) Trace element abundances in rutiles from eclogites and associated garnet mica schists. *Chem. Geol.* **184**, 97–122.

Zajacz Z., Halter W. E., Pettke T. and Guillong M. (2008) Determination of fluid/melt partition coefficients by LA-ICPMS analysis of co-existing fluid and silicate melt inclusions: controls on element partitioning. *Geochim. Cosmochim. Acta.* **72**, 2169–2197.

Zajacz Z., Candela P. A. and Piccoli P. M. (2017) The partitioning of Cu, Au and Mo between liquid and vapor at magmatic temperatures and its implications for the genesis of magmatic-hydrothermal ore deposits. *Geochim. Cosmochim. Acta.* **207**, 81–101.

Associate editor: Horst R. Marschall